INVESTIGATION OF IRE1 AND JNK SIGNALING PATHWAYS IN DSS-INDUCED ER STRESS IN THE MOUSE CEREBRAL CORTEX

A THESIS SUBMITTED TO
THE GRADUATE SCHOOL OF ENGINEERING AND SCIENCE
OF BILKENT UNIVERSITY
IN PARTIAL FULFILLMENT OF THE REQUIREMENTS FOR
THE DEGREE OF
MASTER OF SCIENCE
IN
NEUROSCIENCE

By
Sanem Sobacı
January 2025

INVESTIGATION OF IRE1 AND JNK SIGNALING PATHWAYS IN DSS-INDUCED ER STRESS IN THE MOUSE CEREBRAL CORTEX

By Sanem Sobacı
January 2025

We certify that we have read this thesis and that in our opinion it is fully adequate, in scope and in quality, as a thesis for the degree of Master of Science.

Michelle Marie Adams (Advisor)

Burcu Ayşen Ürgen

Elif Tuğçe Karoğlu Eravşar

Approved for the Graduate School of Engineering and Science:

Orhan Arıkan

Director of the Graduate School

I dedicate this thesis to all the women whose voices were silenced, whose stories went untold, and whose strength remained unseen.

ABSTRACT

INVESTIGATION OF IRE1 AND JNK SIGNALING PATHWAYS IN DSS-INDUCED ER STRESS IN THE MOUSE CEREBRAL CORTEX

Sanem Sobacı

M.S. in Neuroscience

Advisor: Michelle Marie Adams

January 2025

Endoplasmic reticulum (ER) stress plays a critical role in cellular homeostasis and is implicated in various neurodegenerative diseases. The inositol-requiring enzyme 1 (IRE1) is one of the arms of the unfolded protein response (UPR), which is activated in the presence of ER stress. IRE1 pathway activates c-Jun N-terminal kinase (JNK) downstream under prolonged stress.

This thesis explores the activation of the IRE1 and JNK signaling pathways in the mouse cerebral cortex following DSS-induced colitis, focusing on their roles as markers of ER stress in the context of the gut-brain axis. While DSS-induced intestinal inflammation and ER stress are well-established, neurological effects remain less understood. Employing a murine model, the study explored ER stress markers in the cerebral cortex resulting from intestinal pathology.

Despite evidence of DSS-triggered systemic inflammation and ER stress in intestinal tissues, our study revealed no significant differences in the expression levels of IRE1, p-IRE1, or the p-IRE1/IRE1, nor in JNK, p-JNK, or the p-JNK/JNK

between the control and DSS-treated groups. Additionally, these results are supported with correlational and linear discriminant analyses (LDA).

These findings suggest that acute DSS-induced colitis did not elicit a detectable ER stress response in the mouse cerebral cortex under the conditions used. Possible explanations include tissue-specific reactions to the ER stress, transient activation of the IRE1-JNK pathway that returned to baseline by the time of analysis, or potential survivor's bias. Despite its limitations, this thesis provides a novel investigation into the effects of DSS-induced colitis on ER stress in the cerebral cortex.

Keywords: IRE1, JNK, ER Stress, UPR, DSS-induced colitis, gut-brain axis.

ÖZET

DSS KAYNAKLI ER STRESİN İRE1 VE JNK SİNYAL YOLAKLARININ FARE SEREBRAL KORTEKSİNDE İNCELENMESİ

Sanem Sobacı

Nörobilim Lisansüstü Programı, Yüksek Lisans

Tez Danışmanı: Michelle Marie Adams

Ocak 2025

Endoplazmik Retikulum (ER) stresi, hücresel homeostazda kritik bir rol oynar ve çeşitli nörodejeneratif hastalıklarla ilişkilidir. İnositol gerektiren enzim 1 (IRE1), ER stresinin varlığında aktive olan katlanmamış protein yanıtının (KPY) kollarından biridir. Uzamış stres koşullarında IRE1 yolu, aşağı akışta c-Jun N-terminal kinazı (JNK) aktive eder.

Bu tez, IRE1 ve JNK yolaklarının ER stresi belirteçleri olarak rollerine odaklanırken, DSS ile indüklenen kolit sonrası fare serebral korteksinde bu sinyal yolaklarının aktivasyonunu incelemektedir. DSS ile indüklenen bağırsak inflamasyonu ve ER stresi iyi belgelenmiş olmasına rağmen, bunun nörolojik etkileri daha az anlaşılmıştır. Bu çalışma, murin modeli kullanarak bağırsak patolojisinden kaynaklanan serebral kortekstеki ER stres belirteçlerini araştırmıştır.

DSS kaynaklı sistemik inflamasyon ve bağırsak dokularında ER stresine dair kanıtlara rağmen, çalışmamız kontrol ve DSS ile tedavi edilen gruplar

arasında IRE1, p-IRE1 veya p-IRE1/IRE1 ve JNK, p-JNK veya p-JNK/JNK ekspresyon seviyelerinde anlamlı bir fark bulunmadığını ortaya koymuştur. Ayrıca bu sonuçlar, korelasyonel ve doğrusal ayırma analizleri (DAA) ile de desteklenmiştir.

Bu bulgular, kullanılan koşullar altında akut DSS ile indüklenen kolitin fare serebral korteksinde tespit edilebilir bir ER stres yanıtı oluşturmadığını göstermektedir. Bunun olası açıklamaları, ER stresine karşı dokuya özgü reaksiyonlar, analiz zamanına kadar IRE1-JNK yolunun geçici aktivasyonu ve bazal seviyelere dönmesi veya potansiyel bir hayatta kalma yanlılığı olabilir. Sınırlamalarına rağmen, bu tez DSS ile indüklenen kolitin serebral kortekstekı ER stres üzerindeki etkilerini araştıran orijinal bir çalışma sunmaktadır.

Anahtar sözcükler: IRE1, JNK, ER Stresi, KPY, DSS ile indüklenen kolit, bağırsak-beyin ekseni.

Acknowledgement

First of all, I would like to thank my supervisor, Prof. Dr. Michelle Marie Adams, for allowing me to be part of her research team. Her invaluable mentorship, guidance, and insightful feedback were crucial in refining this research project.

I would like to thank Dr. Bahar Değirmenci and the members of her research group, with special thanks to İlke Sarı and Beliz Uzun, for their kind provision of samples and their invaluable assistance.

I would like to thank the members of my thesis committee, Asst. Prof. Burcu Ayşen Ürgen and Dr. Elif Tuğçe Karoğlu Eravşar for their time and their help.

I am also thankful to my colleagues and fellow scientists in the Adams Lab for their engaging discussions and valuable feedback. I would like to express my appreciation to Naz Mengi Çamur, Ilgım Ardıç Avcı, Serena Aktürk, Naciye Bozkurt, Zeynep Karaer, Fulya Kızıldağ, Seçil Gülden and Büşranur Şeker.

I would also like to express my heartfelt gratitude to my close friends Seçil Gülden and Büşranur Şeker for being extraordinary colleagues and great friends. Meeting them during my master's program was one of the greatest gifts of this experience. Their assistance, patience, and understanding have been invaluable to me throughout this journey.

Looking back on this journey, I feel deeply thankful for the friendships I have forged. Even though we are separated by distance, Alper, Kübra, and Ataberk

have given me strength by offering encouragement, laughter, and a listening ear whenever I needed it. Your friendship has been a constant source of comfort, and I am truly grateful for the bond we share. I would also like to thank Yankı Tandırcıoğlu, Ebru Yalçın, and Ezgi Kabukçu for their friendship and the positive impact you've had on my journey.

Throughout this journey, I have been blessed with the unwavering support and love of my family. I am incredibly grateful to my parents, Fatma and Necdet, and my brother, Yusuf Semi, whose encouragement has been my foundation and source of strength. Your belief in me has helped me face every challenge with confidence. I would also like to express my deep gratitude to my grandmother, Üküye, and great-aunt, Bakiye, as well as my mother-in-law, Gökçen, and father-in-law, Engin, for their constant support, love, and care. Their kindness and presence in my life have been a great comfort, and I am forever thankful for their belief in me.

Finally, I wish to express my deepest gratitude to my husband, Barış. Words are futile devices when it comes to conveying how thankful I am for everything. Your belief in me even when I doubted myself and your constant presence made this accomplishment possible. You have been my unwavering support, my source of strength, and my greatest gift. With you by my side, every challenge was easier to face, and every triumph more meaningful. I will forever treasure your love, your faith in me, and the partnership that has carried me through this journey.

Contents

List of Figures

List of Tables

Chapter 1

Introduction

1.1 The Endoplasmic Reticulum

The Endoplasmic Reticulum (ER) is one of the most crucial cellular organelles present in eukaryotic cells. It is a large and dynamic structure that is responsible for diverse functions in cellular processes, including protein synthesis, lipid metabolism, and calcium storage [1]. The ER consists of an extensive network of membranous tubules and sacs called cisternae, covering the nucleus and extending through the cytoplasm [2].

The rough ER (rER) and the smooth ER (sER) are the two distinguishable regions of ER that differ in certain structural and functional characteristics. The rough ER is associated with the presence of ribosomes on its cytoplasmic surface, and these ribosomes specialize in polypeptide synthesis [3]. Upon the synthesis of the proteins, they are directed to the ER lumen for further processing, such as folding and post-translational modification, and then sent to their specific final destinations[4]. Some proteins, for example, remain within the ER, whereas others are further processed in the Golgi apparatus and then directed to the lysosomes or the cell membrane, and some others are secreted from the cell [5].

Smooth Endoplasmic Reticulum, on the other hand, is distinguished from rough ER by its lack of ribosomes. It contributes to lipid synthesis and metabolism and plays a role in the production of new cellular membranes by synthesizing cholesterol and phospholipids [6]. Smooth ER is involved in the production of steroid hormones from cholesterol in specific cell types. Moreover, the detoxification of drugs and harmful chemicals in the liver is conducted by sER [7]. Another function of sER is that it regulates the calcium ion concentration in muscle cells as the sarcoplasmic reticulum, which is important for muscle contraction and signal transduction [8].

1.1.1 Functions of Endoplasmic Reticulum

The Endoplasmic Reticulum is the largest organelle in the cell, and it performs many essential cellular operations. ER is responsible for protein synthesis and protein folding, degradation of misfolded proteins, lipid synthesis, calcium storage and regulation, and glucose metabolism in the cell [9].

1.1.1.1 Protein Synthesis and Folding

Even though protein synthesis can happen in the free ribosomes in the cytosol, synthesis of the secretory and transmembrane proteins, along with a small portion of cytosolic proteins, mainly occurs in the rER [10]. Translation starts in the cytosol, and then ribosomes are recruited to the cytosolic surface of the ER, where the nascent polypeptides with N-terminal signal recognition particle (SRP) are translocated into the ER lumen via translocon membrane channels [11]. After synthesis, ER chaperones and folding enzymes help the proteins undergo folding

and post-translational modifications, such as N-linked glycosylation, disulfide bond formation, and oligomerization [12]. The protein will be transferred inside the cell or the membrane if it is a cytosolic or a membrane protein. On the other hand, secretory protein will continue to be processed in the Golgi apparatus or in the peroxisome for further trafficking to a final destination [13]. These processes are important for proteins to become fully functional in cellular processes or secretion.

1.1.1.2 Degradation of Misfolded Proteins

The process of protein folding is highly controlled with several proteins and complexes, even then, some proteins might be misfolded or unfolded [14]. To prevent aberrant proteins from entering the secretory pathway, these proteins are retained in the ER lumen and degraded with a quality control mechanism called Endoplasmic Reticulum Associated Degradation (ERAD). Misfolded or unfolded proteins undergo ubiquitination and are subsequently degraded by the proteasomes [15].

1.1.1.3 Lipid Synthesis

While rough ER is known as the protein synthesis factory, lipid synthesis is conducted in smooth ER. Phospholipids and cholesterol are synthesized in the ER, especially in the mitochondria and Golgi apparatus contact sites [16]. Also, ER takes place in membrane formation by changing the lipid composition in the lipid bilayer [17].

1.1.1.4 Calcium Storage and Regulation

Calcium ions play important roles as secondary messengers in diverse signaling pathways. Therefore, the regulation and storage of calcium is crucial for cells. The major site for intracellular calcium storage is the ER [18]. Calcium-binding proteins inside the ER lumen sequester calcium ions to maintain low cytosolic calcium concentrations. However, calcium can be rapidly released from ER to the cytosol through channels such as the 1,4,5-trisphosphate receptor (IP_3R) and ryanodine receptor (RyR) in response to cellular signals [19]. It can affect diverse processes both inside the ER, such as proper protein folding, and inside the cell, such as muscle contraction, neurotransmitter release, and even apoptosis [20].

1.2 ER Stress

As mentioned above, one of the main functions of ER is polypeptide synthesis and ensuring the proper folding of these polypeptides. Since protein folding is a highly complex process, it is expected that the misfolding occurs in small proportions. Normally, they can be removed from the ER lumen during routine housekeeping by the ERAD process [21]. This process is known as ER homeostasis and in this balanced state, the demand for protein folding aligns with the protein folding capacity of ER. However, ER stress arises when the misfolded or unfolded proteins accumulate in the ER to the point where the protein folding capacity of the ER gets overwhelmed [22]. Changes in physiological demands, such as disturbances in ER calcium concentrations, osmotic stress, viral infections or toxins can cause increased misfolding of proteins. Moreover, pathological conditions such as cancer,

neurodegenerative diseases and metabolic disorders can lead to increased ER stress [23]. Unfolded protein response (UPR) is an adaptive signaling pathway which helps cells to cope with stress and restore cellular homeostasis. Although ER stress is generally transient and effectively managed by UPR functioning, prolonged ER stress may have lethal effects on cells.

1.3 Unfolded Protein Response (UPR)

UPR tries to relieve stress by increasing the expression of ER chaperons to increase the protein folding levels, as well as decreasing the protein translation. UPR also activates ERAD, which helps to clear misfolded proteins from the ER lumen. Even then, when the ER stress is prolonged, the cell goes into apoptotic cell death mediated by the UPR itself [24].

A series of enzymes and transcription factors are involved in the UPR, as shown in Figure 1. There are three main transmembrane stress sensors: inositol-requiring-enzyme-1 (IRE1), protein kinase RNA (PKR) like ER kinase (PERK), and activating transcription factor 6 (ATF6) [25]. These sensors are responsible for controlling the UPR. These sensors stay inactive when the ER chaperone GRP78 (also called BIP or A5) associates with them. However, the accumulation of misfolded proteins in the ER lumen causes BIP to dissociate from the sensors and activates UPR mechanisms [26].

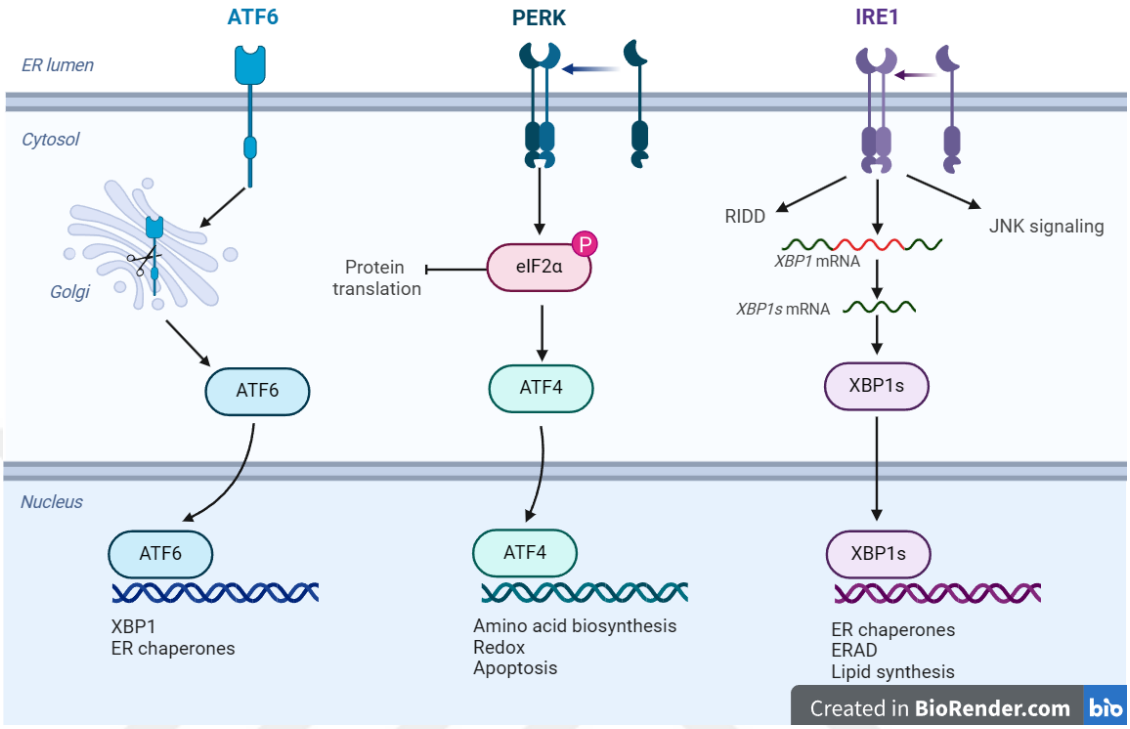

Figure 1. Three stress sensors (IRE1, PERK and ATF6) and downstream pathways as members of UPR. Adapted from "UPR Signaling (ATF6, PERK, IRE1)" by Emma Madden (2024). Retrieved from app.biorender.com/biorender-templates

1.3.1 PERK Pathway

PERK is activated by oligomerization and trans-autophosphorylation after BIP detachment. Following PERK activation, eukaryotic initiation factor-2 (eIF2α) is phosphorylated by PERK, which inhibits the eukaryotic translation initiation factor 2B (eIF2B) activity. These events minimize protein synthesis by arresting the protein translation [27]. Even though eIF2α reduces the initiation of translation, it enhances the transcription factor 4 (ATF4) translation significantly; ATF4 is responsible for regulating the protein synthesis gene expression. It also regulates

the expression of other genes that play roles in pro-survival, such as chaperone proteins or increases the C/EBP homologous protein (CHOP) expression, which is a pro-apoptotic protein. Prolonged stress pushes cells through apoptosis through CHOP regulating the pro-apoptotic and anti-apoptotic proteins [28].

1.3.2 ATF6 Pathway

ATF6 is a transcription factor that belongs to the family of leucine zipper proteins (bZIP). ATF6α and ATF6β are the two different isoforms that are expressed ubiquitously. ATF6 has a different activation pattern from PERK and IRE1. After BIP dissociates from the ER luminal domain of ATF6 in the presence of ER stress, ATF6 relocates to the Golgi apparatus, where the cytoplasmic domain is cleaved. As a result of the cleaving, the N-terminal of the cytosolic segment is translocated to the nucleus and acts as a transcription factor by inducing UPR gene expression. For example, it regulates the expression of chaperons and proteins that take roles in the ERAD pathway to reduce ER stress [29]. Furthermore, ATF6 plays a role in relieving the ER stress by inducing the expression of XBP1 mRNA and CHOP [30].

1.4 IRE1 as a Key Mediator of ER Stress

Inositol-requiring enzyme 1 (IRE1) is the most evolutionarily conserved arm of the UPR both for yeast and mammals. IRE1α and IRE1β are the two paralogues of the IRE1, and they are encoded by ERN1 and ERN2 genes in humans, respectively [31]. The isoforms share 39% similarity in human sequence [15]. It is known that IRE1α is ubiquitously expressed and required for embryonic development. On the other

hand, IRE1β is mainly found in the gastrointestinal tract and lung epithelial cells. Even though IRE1β knock-out animal models suffer from severe colitis, unlike IRE1α, it does not affect the development [32].

IRE1 protein is a ~110 kDa transmembrane protein which possesses dual protein kinase and endoribonuclease (RNase) [33]. Under ER stress conditions, similar to the PERK pathway, BIP disengages due to increased misfolded protein and the ER luminal domain of IRE1 senses these changes, thus IRE1 undergoes dimerization or oligomerization, which enables trans-autophosphorylation [34]. Recent research shows that IRE1 can also sense the unfolded protein increase and activate independently from BIP dissociation [35]. This activation facilitates the cytosolic endoribonuclease domain of IRE1 to act as an RNase and splices a 26-nucleotide intron from the mRNA encoding X-box binding protein 1 (XBP1) [36]. As a result, a spliced isoform of XBP1 (sXBP1) acts as a transcription factor that translocates the nucleus, while an unspliced isoform of XBP1 (uXBP1) becomes unable to activate gene expression. sXBP1 manages a wide range of transcriptions, including the ones involved in ERAD and chaperons to ease ER stress. As well as mitigating ER stress, sXBP1 drives the expression of genes involved in multiple metabolic pathways, for example, lipid biosynthesis, glucose metabolism, DNA repair, cell differentiation, and development [37].

IRE1 RNase cleaves specific sequences of cytosolic mRNAs, ribosomal mRNAs, and miRNAs, but unlike XBP1 cleavage, this one leads to their degradation. This process is called regulated IRE1-dependant decay (RIDD), and it decreases the load of

protein folding, thus ER stress, by reducing protein synthesis [38]. RIDD also causes an inflammatory response due to cleaved mRNA fragments. Therefore, according to the tissue and stress level, RIDD can both play roles in cell survival and cell death [39].

Activation of the protein kinase domain through autophosphorylation not only activates the endoribonuclease domain but is also required for initiating the downstream signaling cascade of c-Jun N-terminal kinase (JNK). Especially, phosphorylations at Ser724, Ser726 and Ser729 domains of IRE1 provide the recruitment of tumor necrosis factor receptor-associated factor 2 (TRAF2) [40]. Apoptotic signaling kinase (ASK1) forms a complex by associating with phosphorylated IRE1 and TRAF2, which leads to the phosphorylation of JNK. JNK activation leads the cell to increased inflammation and apoptosis [41].

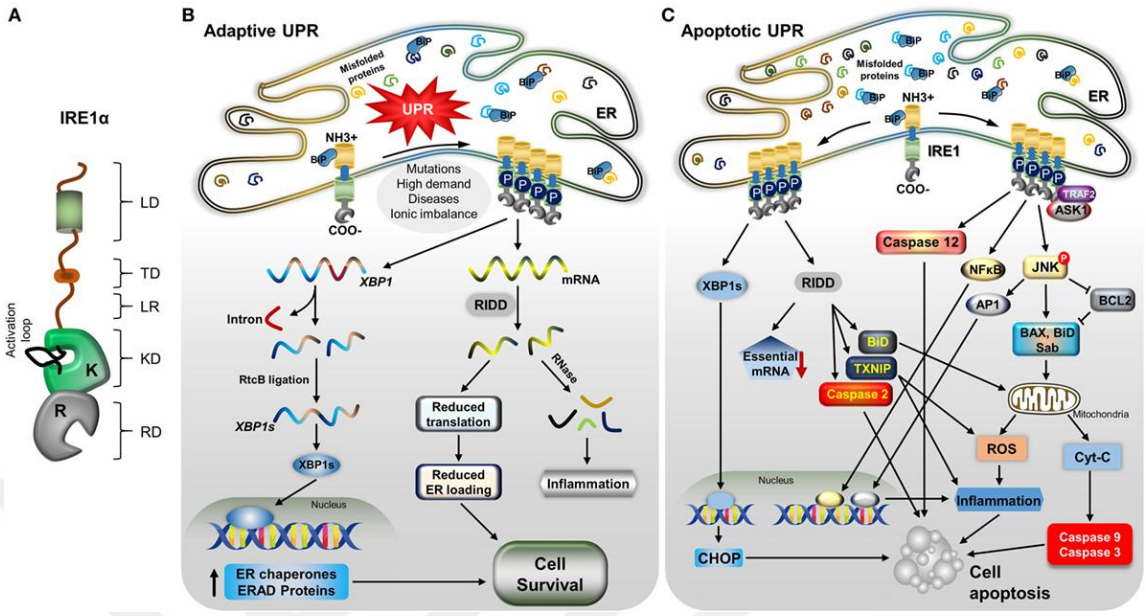

Figure 2. Structure of IRE1 (A) and diverse downstream mechanisms of IRE pathway in cell survival regulated by RIDD and XBP1 (B) and cell death regulated by RIDD and JNK (C) [42].

1.5 JNK Pathway: A Downstream Effector of IRE1

c-Jun N-terminal kinases (JNK), also known as stress-activated kinases (SAPK), are members of the mitogen-activated protein kinase (MAPK) family and play a role in promoting apoptosis as a late ER stress response. JNKs are encoded from three JNK genes, and through alternative splicing, there could be up to ten different isoforms. While JNK1 and JNK2 are expressed throughout all cell types, JNK3 is mainly expressed in the brain [43].

JNK becomes active upon ER stress as a result of phosphorylation by the complex consisting of IRE1, TRAF2 and ASK1. Activation of JNK requires dual

phosphorylation of threonine (Thr183) and tyrosine (Tyr185) motif by mitogen-activated protein kinase kinases (MAP2K), MKK4 and MKK7 [44]. JNK can also be activated when there is an external stimulus by the cell surface receptors. These two activations are somehow similar to each other and JNK mediates cells to go under apoptosis. The mechanism of apoptosis starts with the phosphorylation of Blc-2 and Bim by activated JNK, which inhibits the anti-apoptotic function of Blc-2 and promotes apoptosis. Phosphorylated Bcl-2 cannot bind the pro-apoptotic BH3-only proteins, which induces calcium influx from ER to mitochondria, further driving apoptosis [45].

On the other hand, recent studies show that JNK activation can promote the activation of XBP1 and the expression of several anti-apoptotic genes at the early-stage response to ER stress. However, prolonged ER stress induction causes JNK signaling to become proapoptotic [46].

1.6 Dextran Sodium Sulfate as an Inflammatory Bowel Disorder Model

Inflammatory bowel disorders (IBD) are gut-brain axis disorders characterized by chronic or relapsing gastrointestinal (GI) inflammation. The primary forms of IBD are Crohn's disease (CD) and ulcerative colitis (UC), with symptoms like chronic diarrhea, can even be bloody in severe cases, and pain or discomfort in the abdomen [47]. Chronic inflammation affecting the mucosal layer integrity in the colon is the pathology of UC. On the other hand, CD is characterized by patchy

inflammation that can affect any part of the gastrointestinal tract. Both of them are life-long diseases with active and passive cycles [48].

It is suggested that ER stress can be the primary cause of inflammation in IBD, as well as it could arise as a result of inflammation in the colon. However, it has been shown in both UC and DC subjects that ER stress is comorbid with inflammation [49]. The XBP1 branch of the IRE1 is an important mediator for cell homeostasis, especially for the secretory cells in the intestines. Therefore, reduced XBP1 function causes secretory cell impairment, and it is linked to intestinal inflammation through JNK, which is activated by IRE1 [50].

Even though there are diverse animal models to work on intestinal diseases, such as genetically modified models or adoptive transfer models, chemically induced murine models are one of the most commonly used ones since they are simple to use and more straightforward in controlling the onset, duration, and severity of inflammation. Dextran sulfate sodium (DSS) and trinitrobenzene sulfonic acid (TNBS) have been utilized to induce colitis for over two decades to study IBD. The advantage of DSS-induced colitis is that the acute, chronic or relapsing models can be induced by changing the DSS concentration and administration cycle in mice [51].

1.7 Mouse as an Animal Model

Animal models are crucial for providing insight into complex physiological and pathological processes. Among these models, mice are extensively utilized in research due to their close genetic, anatomical, and physiological similarities to

humans. Their small size, ease of maintenance, and short life cycle are critical elements that provide large-scale studies and expedite the observation of disease progression and treatment outcomes [52].

This study focuses on the gut-brain axis in colitis disease conditions, which is almost impossible to replicate in vitro conditions. On the other hand, the mouse model is effective and versatile while studying multifaceted aspects of the disease models. One of the main advantages of using mouse models is the ability to manipulate their genome. Humanized (gut) models, for instance, can be designed to mimic healthy human gut microbiota. Additionally, the availability of various genetically modified mouse strains permits the investigation of specific genes involved in the gut-brain axis [53].

1.8 Scope of the Study

There are approximately 3 million people in Europe and a growing number of people around the world suffering from inflammatory bowel diseases (IBD). IBD not only impacts individuals' quality of life but also imposes a significant financial strain on healthcare systems [54]. Additionally, patients develop depression and experience cognitive dysfunction over time [55]. It is also known that colitis can alter brain function, affect neurogenesis in the hippocampal region [56], and trigger cortical inflammation in the brain via the gut-brain axis[47].

As mentioned before, ER stress and UPR, especially the IRE1 pathway, play an essential role in maintaining homeostasis in the large intestines, especially in highly

secretory cells. The IRE1-JNK pathway represents a critical axis in determining cell fate during ER stress, balancing adaptive responses with pro-apoptotic signals. Similarly, neurodegenerative disorders have an underlying relationship with the dysregulation of this pathway.

This study aims to advance knowledge of the effects of intestinal inflammation and ER stress that is induced by DSS on the mouse cerebral cortex by focusing on the IRE1 and JNK signaling of ER stress. We also want to explore the activation and interplay of key markers, including IRE1, phosphorylated IRE1 (p-IRE1), JNK, and phosphorylated JNK (p-JNK). This focus allows a detailed examination of ER stress signaling under chemically induced stress conditions, providing insights into cortical tissue-specific responses.

Chapter 2

Materials & Methods

Section 2.1 Animals, Experimental Setup & Ethics, marked with an asterisk (*), was conducted by Bahar Değirmenci Lab Group.

2.1 *Animals & Experimental Setup

18 male C57BL/6 mice subjects, aged 8-12 weeks, used in this study were maintained and handled in the Bilkent University Molecular Biology and Genetics Department Animal Facility. The experimental procedures were conducted in accordance with animal ethics protocols approved by Bilkent University Local Animal Ethics Committee (HADYEK) with decision number 2023/17. Throughout the study, all mice were fed a standard chow diet, and their overall health status was routinely monitored.

During the experiment, the mice were randomly divided into three groups, each consisting of 6 animals. The control group received autoclaved drinking water for a period of 5 days. On the other hand, the mice in the 'DSS-Treatment group' were provided with autoclaved drinking water containing 2.5% dextran sulfate sodium (DSS, MP Biomedicals, CA, USA, 02160110) for 5 days. Both the control and DSS-Treatment groups of mice were sacrificed at the end of the 5 days. Lastly, the

'recovery group' was first administered DSS-containing water for 5 days, after which the water was replaced with autoclaved drinking water for an additional 2 days. These mice were sacrificed at the end of the 7 days.

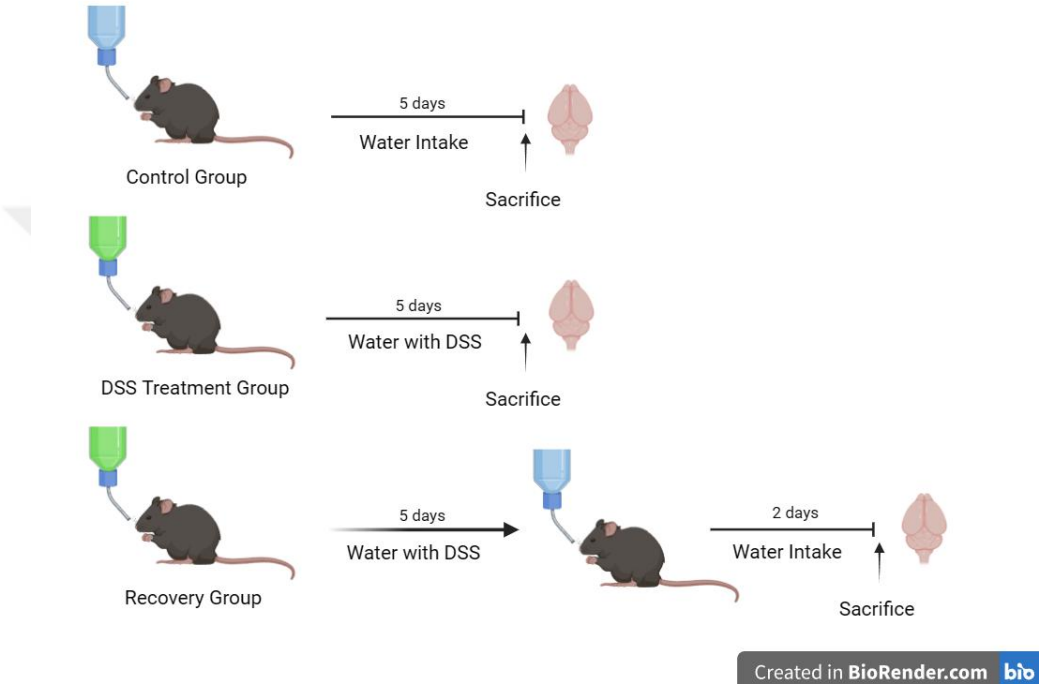

Figure 3. Illustration demonstrating the experimental design for Control, DSS Treatment and Recovery groups**.** The figure is created with BioRender.

2.2 Brain Dissection

Mice were anesthetized in the gas chamber, which contained isoflurane. After 5 minutes, to ensure the animal was anesthetized, the toes of the mouse were pinched. Once there were no reflexes on the toe, the mice were sacrificed using the cervical dislocation technique. The mice were decapitated, and the heads of the mice were washed with alcohol. Subsequently, the skins and the skulls of the heads were cut open, and the whole brains were carefully extracted from a Petri dish by

using forceps and a spatula. Brains were oriented with the ventricular side facing down onto the plate. The following steps were carried out on ice to prevent any protein degradation. To get rid of the excess blood and hair, the brains were rinsed with 0.1 M ice-cold phosphate-buffered saline (PBS).

First, the olfactory bulbs and the cerebella were resected with a scalpel blade. Hypothalami were separated from the rest of the brain using two spatulas. Brains were then divided into two hemispheres from the hemispheric fissure, and the medial sides of the brains were turned to face up. The tissues covering the medial surface of the brains, which were the thalamus, septum, and underlying stratum, were removed for each brain. Next, hippocampi, which are clearly recognizable as banana-shaped structures, were cut off with the help of a spatula. The remaining tissues were the cortex of mice brains.

Hypothalami, Hippocampi, and left and right cortex tissues were collected into 1.5 mL Eppendorf tubes, which were promptly placed in liquid nitrogen to snap-froze the tissues, which prevents protein degradation. Samples were then stored at -80˚C for further use.

2.3 Homogenization of Cortex

The aim of the homogenization process is to disrupt the cell membranes and create a homogenous state of cortex tissues. Frozen right hemispheres of cortex tissues were taken from -80 °C storage and weighed before homogenization. For weighting, the tissues were first taken out of the 1.5 mL Eppendorf tube using a spatula, then

the weights of both the empty Eppendorf tubes and those containing the cortex tissues were measured separately.

Dounce homogenizers were chilled on ice. Approximately 1000 µl of ice-cold PBS was added to each pre-chilled Dounce homogenizer for each tissue. Then, the mice cortex tissues were added to the PBS. The tissues were ground using the pestle's up and down strokes approximately ten times per brain onto the tube. Once the cortex tissues were completely homogenized, the resulting cortex homogenates were transferred into 1.5 mL Eppendorf tubes. To eliminate the remaining particles entirely, the homogenates were passed through a 1 mL 26-gauge needle around ten times, while 1.5 mL Eppendorf tubes were held on ice. The homogenates were then centrifuged at 13000 rpm for 20 minutes at 4 °C. The supernatants were removed as much as possible. Pellets can be stored at -80 °C or used directly for protein extraction.

2.4 Protein Isolation from Mouse Cortex Homogenates

The pellets of mouse cortex homogenates were suspended in 500 µL of ice-cold radioimmunoprecipitation assay (RIPA) buffer containing freshly added protease and phosphatase inhibitors (Table 1). The suspensions were sonicated three times for 5 seconds each at 50 amp for 0.5-1 cycle on ice to break apart the cell membranes effectively. The suspensions were incubated on ice for 30 minutes, and sample tubes were gently mixed by tapping every 10 minutes. Next, the centrifugation was conducted at 13000 rpm for 20 minutes at 4˚C. After the centrifugation, the supernatants were collected into new 1.5 mL Eppendorf tubes.

Supernatants were aliquoted to prevent the degradation of proteins from repeated thaw and freeze cycles.

Table 1. RIPA Buffer Recipe

Stock Solution	**Volume (µL) 1 mL**
2M NaCl	75
1 M Tris HCl pH: 8	50
100% NP-40	10
10% Sodium Dodecyl Sulfate (SDS)	10
Protease Inhibitor Cocktail	10
Phenylmethylsulfonyl Fluoride (PMSF)	10
Sodium orthovanadate (Na_3VO_4)	10
ddH_2O	855

2.5 Bradford Assay

Bradford Assay was employed to measure the unknown concentrations of soluble proteins. This method detects proteins via “Coomassie Brilliant Blue” dye, which binds to the proteins and changes the intensity of the color by producing a blue color. A 96-well plate was utilized for the Bradford Assay, ddH_2O was used as a blank, and Bovine serum albumin (BSA, A7906, Sigma-Aldrich, St. Louis, MO, USA) was used as the standard protein solution.

A series of protein standards with different concentrations ranging from 0 to 1 mg/ml were prepared by diluting the BSA with ddH_2O to generate a standard curve,

and the details are given in Table 2 below. 0.5 µL isolated protein samples were diluted with 4.5 µl ddH_2O and loaded into the 96-well plate. All standard protein solutions, blank, and protein samples were loaded as duplicates to reduce pipetting variations. Then, 250 µL of Bradford Reagent (B6916, Sigma, St. Louis, MO, USA) was added to each well. Subsequently, the solutions were mixed at 240 rpm for 45 seconds at room temperature on an orbital plate shaker. The 96-well plate was then placed in a box covered with an aluminum folio to prevent the plate from being exposed to light. The plate was incubated for 10 minutes at room temperature without shaking to allow the dye to bind to the proteins. Before the measurement, any air bubbles were checked and removed using a sterile syringe tip.

The absorbance of each standard and sample protein was measured at 595 nm using a Synergy HT Multi-Mode Microplate Reader. The blank wells were assigned as “Blank”, and standard proteins and protein samples were chosen as “Sample” from the software. If the absorbance values fell within the range of the standard curve, the absorbance of the blank was subtracted from each sample, and the measurements were recorded as net absorbances. Otherwise, the samples had to be diluted and remeasured. The absorbance values of BSA standards against their protein concentrations were plotted using Excel. Then, the linear regression line was fitted to the data points on the graph, and the equation of this line was used to calculate the protein concentrations of isolated protein samples.

Table 2. Dilutions of BSA Standard Protein Solutions

	ddH_2O (µL)	**BSA (1 mg/1 ml stock) (µL)**	**Final Concentration (µg/µL)**
Blank	5	0	0
Standard 1	4.5	0.5	0.1
Standard 2	4	1	0.2
Standard 3	3	2	0.4
Standard 4	2	3	0.6
Standard 5	1	4	0.8
Standard 6	0	5	1

Table 3. Representative 96-well plate design for Bradford Assay

	1	**2**	**3**	**4**	**5**	**6**	**7**	**8**
A	Blank	Blank	Sample 1	Sample 1	Sample 9	Sample 9	Sample 17	Sample 17
B	Standard 1	Standard 1	Sample 2	Sample 2	Sample 10	Sample 10	Sample 18	Sample 18
C	Standard 2	Standard 2	Sample 3	Sample 3	Sample 11	Sample 11		
D	Standard 3	Standard 3	Sample 4	Sample 4	Sample 12	Sample 12		
E	Standard 4	Standard 4	Sample 5	Sample 5	Sample 13	Sample 13		
F	Standard 5	Standard 5	Sample 6	Sample 6	Sample 14	Sample 14		
G	Standard 6	Standard 6	Sample 7	Sample 7	Sample 15	Sample 15		
H			Sample 8	Sample 8	Sample 16	Sample 16		

2.6 Western Blot

Western Blot, also referred to as immunoblotting or protein blotting, is a commonly used analytical technique to detect the presence of specific proteins in the used sample with the help of specific antibodies. Additionally, since it enables the quantification of the proteins based on the relative thickness of the bands, Western Blot can be used to establish the changes in the protein levels across different treatments [57]. The steps involved in the Western Blot protocol are illustrated in Figure 4.

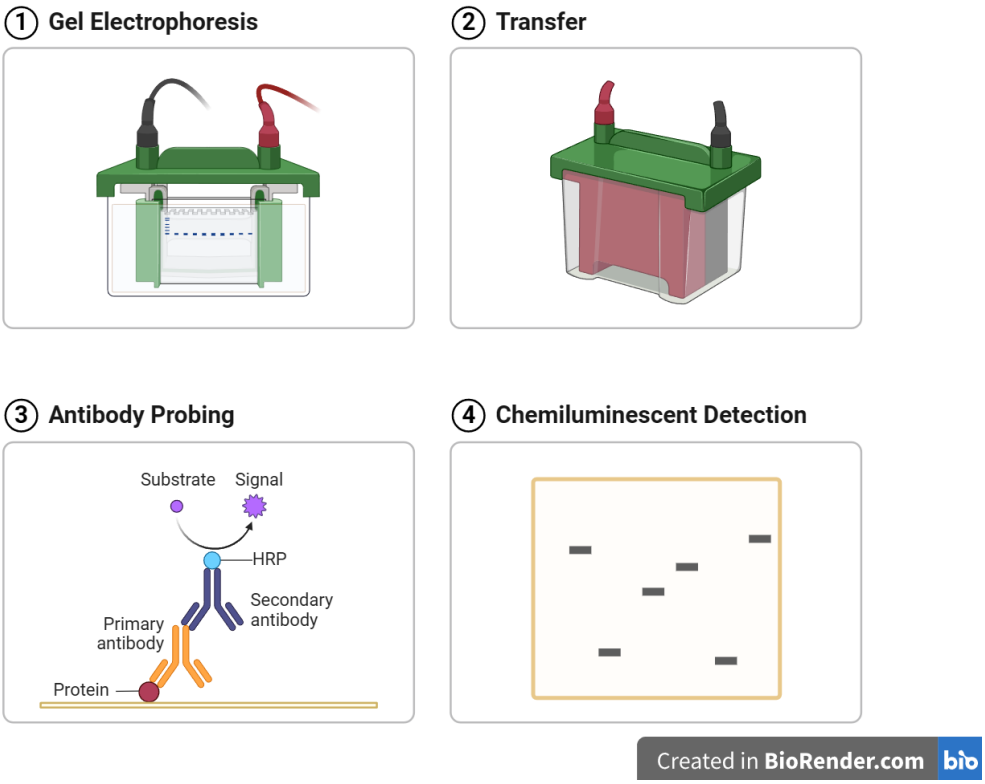

Figure 4. Illustration demonstrating the four main steps of the Western Blot protocol. Adapted from "Western Blotting Workflow" by BioRender.com (2024). Retrieved from app.biorender.com/biorender-templates

2.6.1 Sample Preparation

After the optimization experiments were completed, the protein amount loaded into each well was standardized to 20 µg for all the antibodies to avoid saturation of band intensities. 10% Dithiothreitol (DTT) was added to the 2X Loading Dye (Table 4) just before the sample preparation to break the disulfide bonds in the proteins. According to the results of the Bradford Assay, concentrated proteins were diluted with ddH_2O to a final volume of 10 µL and then mixed with 10 µL of 2X Loading Dye containing DTT. The samples were incubated at 95˚C in the heater for 10 minutes to denature proteins, and then allowed to cool down before being loaded into the wells or stored at -20 °C until further use.

Table 4. 2X Loading Dye Recipe

Solutions	**Volume 20 mL**
10% SDS	8 mL
100% Glycerol	4 mL
4% Bromophenol Blue	250 µL
1 M Tris-HCl (pH 6.8)	2 mL
ddH_2O	up to 20 mL

2.6.2 SDS-PAGE Gel Preparation

The stacking gel was prepared with a polyacrylamide concentration of 5%, while a 10% separating (or resolving) gel was selected according to the molecular weights of the proteins of interest, ranging from 130 kDa to 40 kDa. The chemicals listed in

Table 5 and Table 6 were combined in specified quantities to prepare the stacking and separating gels, respectively. All the chemicals, except Ammonium persulfate (APS) and N,N,N'N'-tetramethylethane-1,2-diamine (TEMED), were added to both gel solutions.

The short glass plate was positioned atop the 1.5 mm spacer plate, and both plates were inserted into the green casting frame with the short plate facing forward on a flat surface. After both plates were evenly aligned at the bottom, the casting frame was clamped. The possible leakage was tested by pouring dH_2O before pouring gels between the glass plates. Once it was confirmed that there was no leakage in the gel cassettes, the water was removed, and the space between the glass plates was dried with the help of Watman Filter Paper.

When the gel cassettes were ready, APS and TEMED were quickly added to the 10% separating gel, mixed by inversion, and poured between the glass plates, filling the space to about 1.5 cm below the short plate. A layer of isopropanol was added on top of the separating gel in order to eliminate bubble formation and level the surface of the gel. The gel was left to polymerize for around 25 minutes, which was ensured by checking the remaining prepared gel. Once the separating gel had polymerized, the isopropanol was carefully removed, and the area was dried with Whatman Paper, avoiding contact with the gel surface.

APS and TEMED were then added to the 5% polyacrylamide stacking gel, which was gently mixed before being poured onto the separating gel between the glass plates. A 15-well 1.5 mm comb was carefully placed on top of the gel, removing bubbles if

there were any. Again, the polymerization process took approximately 25 minutes. The gel could be used immediately or stored for up to a week in a sealed plastic bag or between plastic foil with dH_2O wetted towels at 4˚C.

Table 5. 10 % Separating Gel Recipe for 2 Gels

Solutions	Volume
ddH_2O	7.08 mL
1 M Tris HCl (pH 8.8)	7.54 mL
10% SDS	200 µL
40% Acrylamide	5 mL
10% APS	200 µL
TEMED	20 µL

Table 6. 5 % Stacking Gel Recipe for 2 Gels

Solutions	Volume
ddH_2O	7.54 mL
1 M Tris HCl (pH 6.8)	1.25 mL
10% SDS	100 µL
40% Acrylamide	1 mL
10% APS	100 µL
TEMED	10 µL

2.6.3 SDS-PAGE Gel Electrophoresis

SDS-PAGE Gel Electrophoresis aims to separate proteins based on their molecular weight by applying an electrical current. Mini-PROTEAN® Tetra Cell (BioRad, CA, USA) system was used for electrophoresis. First, both gel sandwiches were clamped to the electrode assembly module, ensuring that the short plates faced inward. The electrophoresis module was then placed into the tank, and any leakages were checked by filling it with fresh 1X Running Buffer, which was prepared by diluting 10X Running Buffer (Table 7) with distilled water. If excessive leakage was detected, the gel sandwich alignment on the gel supports at the bottom of the clamping frame assembly needed to be checked. After that, the tank was filled with either used or fresh 1X Running Buffer up to the blotting or four gels level.

Following the gentle removal of the combs, the wells were rinsed with 1X Running Buffer. The samples were briefly spun using QuickSpin Mini Centrifuge and mixed. Then, 1.5 µL PageRuler Prestained Protein Ladder (6619, Thermo Scientific, 10-250 kDa) was loaded into the first and last wells to accurately estimate the molecular weight of the proteins. Moreover, it provided real-time monitoring of the electrophoresis progress since each protein band in the ladder has different colors. 18 µL of 20 µg protein samples were loaded into each well carefully. Each gel contained four cohorts, and the same sample sequence was loaded for gels run on the same tank to assess the relative level of phosphorylation of the proteins accurately.

Once all samples were loaded, the tank lid was closed by assembling the colors of the banana plugs on the electrode assembly. The jacks on the tank lid and electrical leads on the lid were inserted into the power supply. The electrophoresis was conducted at 80 volts for around 30 minutes so that samples could properly align for separation. The voltage was then increased to 100 volts for approximately 130-150 minutes, until the sample loading dyes reached the bottom of the gel.

Table 7. 10X Running Buffer Recipe

Solutions	**Volume 1 L**
Tris Base	30.285 g
Glycine	144.134 g
10% SDS	100 mL
dH_2O	up to 1 L

2.6.4 Electrophoretic Protein Transfer

Protein transfer provides immobilization to the proteins by transferring them to a stable and solid surface, such as nitrocellulose or polyvinylidene fluoride (PVDF) membranes. The Mini Trans-Blot Cell system (BioRad, CA, USA) was employed for the electrophoretic protein transfer. Polyvinylidene fluoride (PVDF, Thermo Scientific™) transfer membranes with a 0.45 µm pore size were labeled on the right side and activated in 100% methanol for a minimum duration of one minute. The membranes were then immersed in 1X ice-cold fresh Transfer Buffer with freshly added methanol (Table 8). As well as the Whatman filter papers and foam pads

were presoaked into the 1X used ice-cold transfer buffer during the final 10 minutes of electrophoresis.

Table 8. 1X Transfer Buffer Recipe

Solutions	**Volume 1 L**
Tris Base	3.02 g
Glycine	14.4 g
dH_2O	up to 800 ml
100% Methanol	200 ml

To prepare the blotting sandwiches, gel holder cassettes were positioned with their black sides facing down in a tray containing 1X Transfer Buffer. Then, presoaked fiber pads were first placed on the black side, followed by two layers of Whatman filter papers. Upon completion of the gel electrophoresis, the gel sandwiches were carefully removed from the gel cassette, and the short plates were separated with the help of a gel releaser. The stacking gels were discarded, and the gels were placed onto the Whatman Papers. Pre-soaked PVDF membranes were placed on the gels. After placing one layer of Whatman Paper, air bubbles trapped between the gels and the membranes were meticulously removed. Subsequently, another layer of Whatman Paper and a fiber pad were added to complete the blotting sandwich, as illustrated in Figure 5. The blotting sandwiches were then closed and secured with the sliding clamp. The gel holders were inserted into the inner module, ensuring that the black side of the gel holders faced the black side of the module. The module was then placed into the transfer tank, a frozen cooling unit was added

to the tank, and the tank was filled with ice-cold 1X Transfer Buffer up to the blotting line. The lid was attached according to the color code, and the leads were connected to the power supply. The protein transfer was conducted in a cold room for 90 minutes at 100 volts.

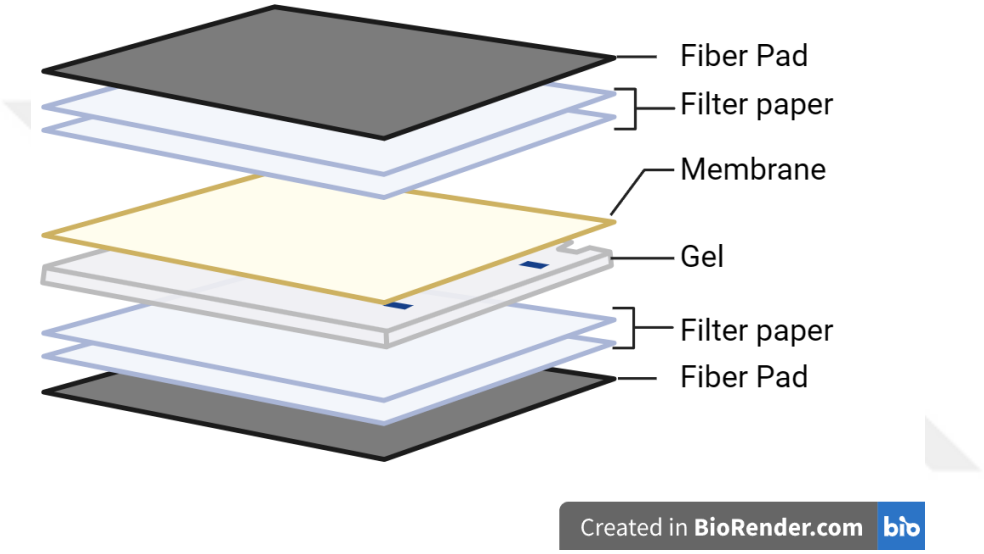

Figure 5. The figure represents the blotting sandwich system of Western Blot Electrophoretic Protein Transfer. Adapted from "Membrane Transfer Schematics" by BioRender.com (2024). Retrieved from app.biorender.com/biorender-templates

2.6.5 Blocking, Primary and Secondary Antibody Probing

Blocking is an essential step aimed at preventing the non-specific binding of antibodies to the membrane, thereby improving the clarity of the results by reducing background noise. The 10X Tris-buffered saline (TBS) was prepared based on Table 9. Then, it was diluted to 1X, and 0.1% Tween 20 was added to prepare 1X TBS-Tween-20 (TBS-T), which was used as the washing solution. The blocking

solutions were prepared in advance during the protein transfer stage, and their composition was determined through prior optimization experiments. Specifically, 5% w/v non-fat dry milk in 1X TBS-T, and 5% w/v BSA in 1X TBS-T were freshly prepared. Following the completion of protein transfer, the PVDF membranes were taken from the blotting sandwiches, placed upwards, and wetted with TBS-T on a clean and even surface. To allow the detection of two distinct antibodies on each membrane, the membranes were horizontally cut at the level corresponding to the 70 kDa protein marker. Subsequently, the membranes were immersed in their respective blocking solutions and incubated for 1 hour at room temperature with gentle agitation.

Table 9. 10X Tris-Buffered Saline Recipe, pH 7.6

Solutions	**Volume** **1 L**
Tris Base	24 g
Sodium Chloride (NaCl)	80 g
dH_2O	up to 1 L

At the end of the blocking step, the membranes were briefly rinsed with 1X TBS-T. The membranes were then incubated with the appropriate primary antibodies, including anti-IRE1α (14C10) (1:1000, Cell Signaling #3294), anti-IRE1 (phospho S724) [EPR5253] (1:1000, Abcam ab124945), anti-SAPK/JNK (1:1000, Cell Signaling #9052), Phospho-SAPK/JNK (Thr183/Tyr185) (81E11) (Cell Signaling #4668) and anti-β-Tubulin (1:5000, Cell Signaling #2146), all diluted to target

specific concentrations, the details were given in Table 10. Overnight incubations were carried out at 4˚C cold room with gentle agitation.

Table 10. Detailed list of primary antibodies used in Western Blot Experiments

Antibody Name	Specifications	Dilution	Dilution Solution	Blocking Solution	Secondary Antibody
IRE1α	Cell Signaling Technology, #3294	1:1000	5% BSA in TBS-T	5% milk in TBS-T	Rabbit HRP in 5% milk in TBS-T
IRE1 (phospho S724)	Abcam, ab124945	1:1000	5% BSA in TBS-T	5% BSA in TBS-T	Rabbit HRP in 5% BSA in TBS-T
SAPK/JNK	Cell Signaling Technology, #9052	1:1000	5% BSA in TBS-T	5% milk in TBS-T	Rabbit HRP in 5% milk in TBS-T
Phospho-SAPK/JNK	Cell Signaling Technology, #4668	1:1000	5% BSA in TBS-T	5% BSA in TBS-T	Rabbit HRP in 5% BSA in TBS-T
β-Tubulin	Cell Signaling Technology, #2146	1:5000	5% BSA in TBS-T	5% milk in TBS-T	Rabbit HRP in 5% milk in TBS-T

The next day, upon completion of the primary antibody incubation, primary antibodies were collected to their falcons for further use. The membranes were then subjected to three consecutive washes with 1X TBS-T, each lasting 10 minutes, to remove any unbound primary antibodies. Subsequently, the membranes were incubated with diluted anti-rabbit IgG, Horseradish Peroxidase (HRP)-conjugated secondary antibody (1:5000, Cell Signaling #7074) for all primary antibodies for 1 hour at room temperature on a shaker with gentle agitation. Lastly, the secondary

antibodies were collected, and the membranes were washed three times with 1X TBS-T for 10 minutes to ensure the removal of excess antibodies.

2.6.6 Chemiluminescent Detection

Chemiluminescent detection is a highly sensitive visualization method that relies on the emission of light through chemical reactions. For this process, SuperSignal™ West Femto Maximum Sensitivity Substrate (34095, Thermo Scientific, Rockford, IL, USA) was utilized as the chemiluminescent substrate. Following the manufacturer's instructions, a 1:1 mixture of the Luminol/Enhancer solution and Stable Peroxide Buffer was prepared in an Eppendorf tube, which was shielded from light using aluminum foil to prevent premature exposure. The membrane was then placed on a clean, flat surface, and the prepared substrate solution was evenly applied to cover the entire membrane. Upon 2 minutes of incubation in the dark, the membrane was covered with transparent plastic to prevent the membrane from drying. Subsequently, the membrane was placed inside the ChemiDocTM XRS+ imaging system (Biorad, CA, USA), where the images were captured using ImageLab software (Biorad, CA, USA), ensuring optimal setting and appropriate exposure times for each membrane.

2.7 Band Intensity Quantification

After the images were saved, they were exported from ImageLab as tiff files. To avoid any biases during quantification, the images were quantified by Zeynep Karaer. The ImageJ program (NIH, Bethesda, MD, USA) was used to quantify the band intensities. The tiff files were opened in ImageJ software, and a rectangle was

drawn around the first lane by using the rectangular selection tool. The area of the lane above and below the band of interest was enclosed and select first lane command was selected. Then, the rectangle was moved over the next lanes and the following bands were selected with the select next lane command. Upon completing all bands, the lanes were plotted. At the base of each peak, a line was drawn from one side of the peak to the other with the help of the straight line selection tool. To calculate the area under the peaks for each band, the area inside the peaks was chosen with the wand tracing tool [58]. One exception during the process was the p-SAPK/JNK antibody results. There were three bands for this antibody, but the middle band was nonsignificant. Therefore, only the areas under the peaks of upper and lower bands included the quantification. The results were then exported to an Excel sheet.

To be able to lower the effect of experimental conditions, first gel normalization was performed by dividing each band density by the average band density for each antibody. Following the gel normalization, the loading control protein normalization was performed in a similar way. The normalized gel value of each protein was divided by the normalized gel value of the housekeeping protein, which is β-tubulin, on the corresponding lane. After proteins were normalized according to their own housekeeping protein values, the normalized phospho-protein value was divided by the normalized total value of the specific antibody for the phosphorylated proteins. Upon completing the loading control protein normalization, two technical replicates were calculated by taking the average of two values for each protein, and the final results were used in the statistical analysis.

2.8 Statistical Analysis

After the gel normalizations, the statistical analyses were done in IBM SPSS Statistics 26.0 (Armonk, NY, USA), GraphPad Prism 10 (Boston, USA), and Python (Rossum, Amsterdam, Netherlands). Shapiro-Wilk test was used to test normality and Levene's test for the homogeneity of the variance. Two of the three treatment groups, control and DSS-treatment, each for 6 biological replicates were included in the statistical analysis. A non-parametric Mann-Whitney U test was conducted for the ones which failed the assumption of normality, and the rest of the protein expression was tested with independent samples T Test. On the other hand, analysis of the recovery group with other groups contained one-way ANOVA for the normally distributed samples and Kruskal Wallis for the rest. The recovery group analyses were added to Appendix A since its lack of control group. Statistically significant value was accepted as $*p \leq 0.05$.

Additionally, after the normality of the data set was assured using the Shapiro-Wilk test, the Pearson correlation test was conducted to find linear correlations between IRE1α, p-IRE1α, p-IRE1/IRE1, JNK, p-JNK, p-JNK/JNK. Then, Linear Discriminant Analysis (LDA) was performed to detect the separability between control and DSS-treatment groups. The LDA model was trained using the Python scikit-learn library. The feature matrix consisted of IRE1, JNK, p-IRE, and p-JNK, while the target vector represented the group labels.

Chapter 3

Results

3.1 Optimizations for Western Blot

Optimization Western blot experiments were conducted to determine the best parameters for optimal detection of the protein expression of the IRE1α, p-IRE1, JNK, and p-JNK antibodies, as well as XBP1s (BioLegend #619502). The Western blot results revealed distinct bands corresponding to the molecular weights of the target proteins, confirming their expression.

For IRE1α, using Neuro-2A Control Extract as a positive control confirmed the protein's expected molecular weight, with a single band at approximately 130 kDa observed in both the cortex homogenates and the control. For the phosphorylated form, IRE1 (phospho S724), the first antibody tested (Abcam ab48187) produced double bands near the expected 110 kDa. However, the presence of a double band prompted a switch to another antibody, anti-IRE1 (phospho S724) [EPR5253] (Abcam ab124945) was optimized for the experiments. This adjustment yielded the expected single band at 110 kDa, confirming the successful detection of the phosphorylated protein.

For JNK and p-JNK, the bands were expected to be observed at 46 kDa and 54 kDa, representing the two isoforms of the protein. JNK bands were detected as expected. On the other hand, Phospho-SAPK/JNK (Thr183/Tyr185) (G9) (Cell Signaling #9255), the detection results were suboptimal, as two clear bands were not consistently observed. To address this issue, Phospho-SAPK/JNK (Thr183/Tyr185) (81E11) (Cell Signaling #4668) was tested along with a positive control, 293+ UV Control Extract. Even though this adjustment improved the specificity and clarity of the results, a third band was consistently observed between the bands at 46 kDa and 54 kDa. After thorough research and literature review, this band was determined to be a non-specific signal and was therefore excluded from the quantification process. The focus was maintained on the two expected bands corresponding to the 46 kDa and 54 kDa isoforms of JNK and p-JNK.

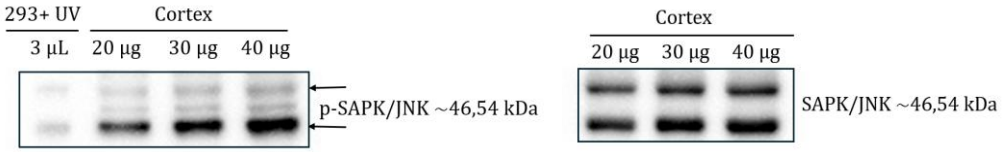

Figure 6. Representative Western Blot images of optimization for JNK and p-JNK protein using mouse brain homogenates. 293+ UV: 293 cell lines treated with UV light used a positive control.

In contrast, for XBP1s, although a band at 54 kDa was anticipated, no bands were observed in the optimization experiments. This is due to the incompatibility of the antibody with brain tissue. Therefore, XBP1s cannot be used for experimental tissue.

To determine the appropriate protein loading amount for optimal band intensity, cortex homogenates were loaded onto the gel in quantities of 20 µg, 30 µg, and 40 µg. The resulting band intensities for IRE1α, p-IRE1, JNK, p-JNK, and β-tubulin were analyzed, and saturation curves were generated for each protein. Based on these curves, 20 µg of protein was selected as the optimal loading amount to ensure sufficient band intensity while avoiding oversaturation. This standardized loading protocol was subsequently used in all experimental Western blots to maintain consistency and reliability in quantification.

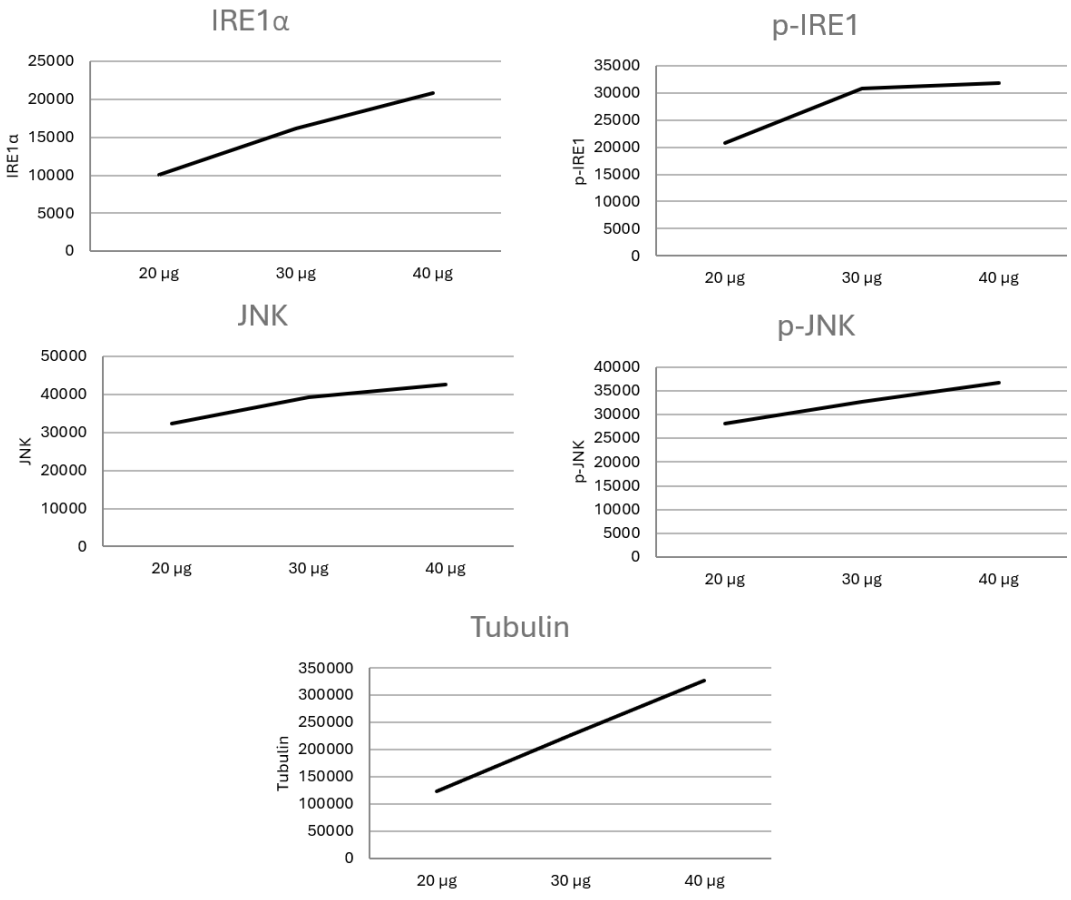

Figure 7. Saturation Curve Graphs for all protein used in this experiment.

3.2 The Effect of DSS Treatment on p-IRE1α in Mouse Cerebral Cortex

To assess the activation of IRE1α, the levels of both IRE1α and its phosphorylated form (p-IRE1α) were measured. The phosphorylation or activation levels of IRE1α were then determined by calculating the ratio of p-IRE1α to IRE1α. The normality and heterogeneity of the data were checked by Shapiro-Wilk and Levene's Tests, respectively. Mann Whitney-U test has revealed that DSS treatment does not have a significant effect on the expression level of p-IRE1α ($U_{(X)}$ = 22.000, p = 0.589). Also, the independent samples T Test has shown that DSS treatment does not have a significant change on neither the IRE1α protein expression ($t_{(10)}$ = -0.574, p = 0.579) nor the ratio of p-IRE1α to IREα ($t_{(10)}$ = 0.379, p = 0.712), as can be seen in Figure 6.

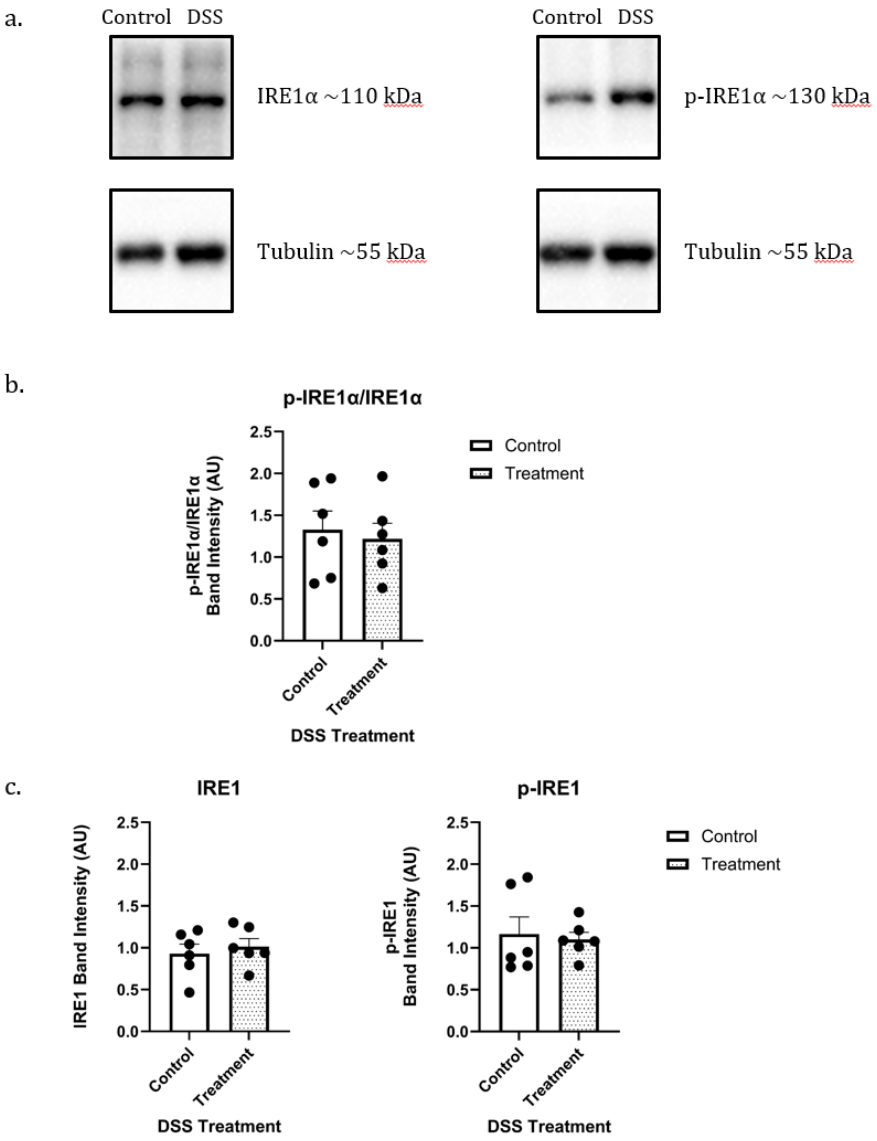

Figure 8. Expression Levels of IRE1α, p-IRE1α and the Ratio of p-IRE1α/ IRE1α across all groups in Cerebral Cortex. The representation of Western Blot bands for IRE1α, p-IRE1α, and as a housekeeping protein Tubulin (a). The graph shows the normalized quantification of the p-IRE/IRE1α ratio for control and DSS treatment groups (b). Lastly, the expression levels of IRE1α (left) and p-IRE1 (right) across DSS treatment groups are shown in c. The error bars represent mean +1 SEM. n=6 for all groups.

3.3 The Effect of DSS Treatment on p-JNK in Mouse Cerebral Cortex

Both the quantification of normalized bands of JNK and phosphorylated JNK (p-JNK) were taken into account to measure the activation levels of JNK, which is found by taking the p-JNK/JNK ratio. Shapiro-Wilk test is applied for normality, and Levene's test is for heterogeneity. Mann Whitney-U test has revealed that DSS treatment does not have a significant effect on the ratio of expression levels of p-JNK to JNK ($U_{(X)}$ = 19.000, p = 0.873). Additionally, the independent samples T Test has revealed that DSS treatment does not have a significant effect on the JNK expression ($t_{(10)}$ = -1.186, p = 0.263) and on p-JNK levels ($t_{(10)}$ = -0.621, p = 0.549), the graphs are shown in Figure 7.

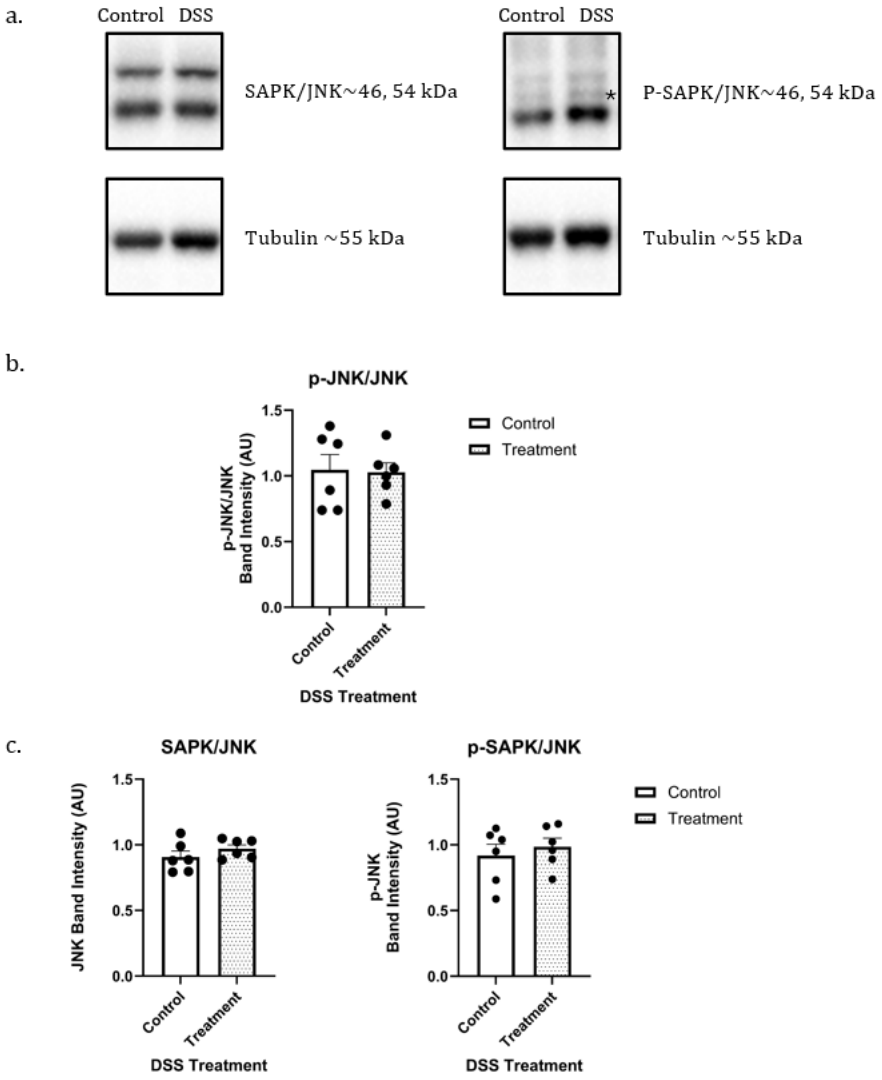

Figure 9. Expression of JNK, p-JNK and the Ratio of p-JNK to JNK across all groups in Cerebral Cortex. The representation of Western Blot bands for JNK, p-JNK, and Tubulin as a housekeeping protein (* represents the non-significant band) (a). The graph represents the normalized quantification of p-JNK to JNK ratio for control and DSS treatment groups (b). The expression levels of normalized JNK (left) and p-JNK (right) band quantifications across DSS treatment groups (c). The error bars represent mean +1 SEM. n=6 for all groups.

3.4 Correlation Analysis of IREα and JNK Activation

A correlational analysis was conducted to explore the relationships among IRE1α, p-IRE1α, the ratio of p-IRE1α to IRE1α, JNK, p-JNK, and the ratio of p-JNK to JNK. To observe the overall correlation and clustering profiles between these proteins, they were analyzed without the group's effects. Then, the correlation analysis was conducted separately within the control and DSS-treatment groups. The normality for these correlation groups was checked by the Shapiro-Wilk test. Pearson correlation was performed for each, and the correlations were shown in Figure 8 below as heatmap graphs. The color intensity and direction (red for negative, blue for positive) represent the strength and polarity of correlations, respectively. Statistically significant value was accepted as *p≤0.05.

A significant negative correlation between p-IRE1/IRE1 and IRE1α can be observed in Overall (r = -0.70, p = 0.011), and DSS-Treatment (r = -0.90, p = 0.015) groups. Similarly, a positive correlation between p-JNK/JNK and p-JNK is significant in Overall (r = 0.87, p = 0.000), Control (r = 0.90, p = 0.013) and DSS-Treatment (r = 0.89, p = 0.017) groups. IRE1α and p-JNK showed a significant correlation in Overall (r = 0.57, p = 0.054).

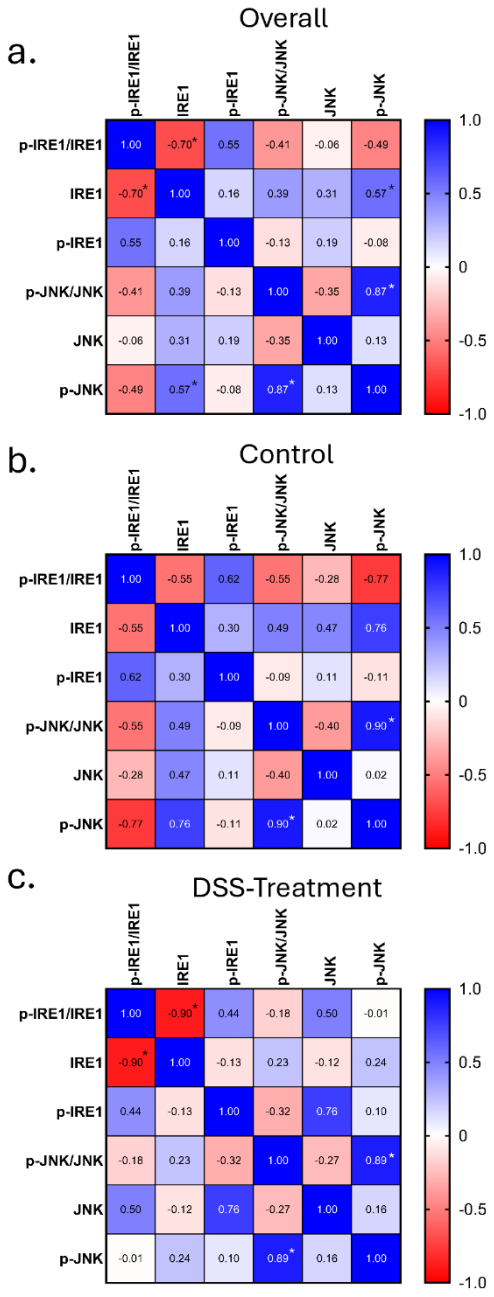

Figure 10. Correlation Heatmap Graphs between IRE1α and JNK Protein Expressions. Heatmaps represent the overall correlation (a), correlation only for the control group (b), and correlation analysis only for the DSS-Treatment group (c). r = 1 or -1 represents a strong correlation, r = 0 represents no correlation. *p≤0.05.

3.5 Linear Discriminant Analysis (LDA)

Two separate linear discriminant analyses were performed to observe separability between control and DSS-Treatment groups. First LDA was conducted between IRE1α, p-IRE1, JNK, and p-JNK. The absolute values of the coefficients were computed to determine the percentage contribution of each feature. The results indicate that JNK had the largest positive coefficient at 7.680 and contributed the most to LD1, with a percentage contribution of 75.64%. In contrast, p-IRE1 had a negative coefficient at -0.883, contributing 8.70% to LD1, implying that its variation opposes the dominant direction defined by JNK. p-JNK contributed positively with a coefficient of 1.386 and a percentage contribution of 13.66%. IRE1α had the smallest coefficient of 0.202 and the lowest percentage contribution with 1.99%. Their coefficient values and percentage contributions of these values to the first linear discriminant (LD1) were shown in Table 11.

Table 11. LD1 Coefficients and Percentages for the IRE1α, p-IRE1, JNK and p-JNK

	LD1 Coefficients	**Percentage Contributions**
JNK	7.680	75.64
p-JNK	1.386	13.66
p-IRE1	-0.883	8.70
IRE1α	0.202	1.99

The second LDA was conducted only to check the separability of the activation of the proteins by checking the p-IRE1/IRE1 and p-JNK/JNK ratios between the control and DSS-Treatment groups. Both coefficients are negative, p-IRE1/IRE1 contributes with a coefficient of -0.599, and p-JNK/JNK shows a slightly greater magnitude with -0.836.

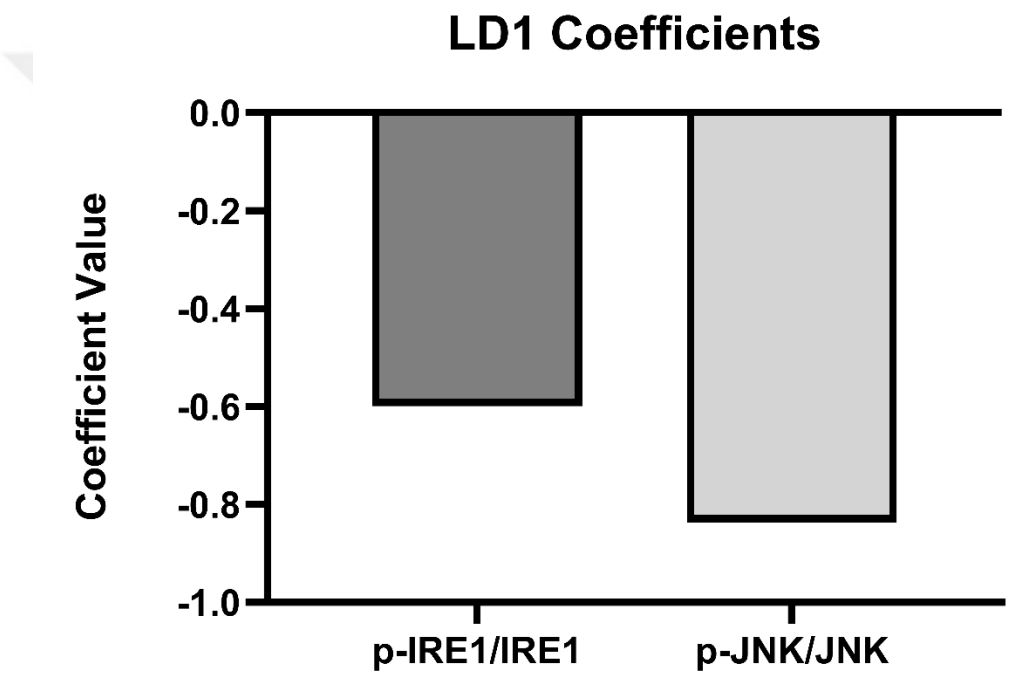

Figure 11. The bar plot displays the LD1 coefficients for the p-IRE1/IRE1 and p-JNK/JNK ratios.

Chapter 4

Discussion

ER is an important player in maintaining cellular homeostasis since it is responsible for crucial tasks such as protein folding, lipid biosynthesis, and calcium storage in the cell. Maintaining homeostasis in the brain is especially vital for neuron function, survival, and plasticity. Disruption of the balance state of ER by the accumulation of misfolded proteins triggers the UPR, which tries to restore the balance at the early stages, but prolonged stress triggers cell death via apoptosis. When the ER stress becomes chronic, pro-apoptotic signals like JNK lead neurons to apoptosis, which contributes to the neurodegenerative processes [59]. Additionally, alterations in the UPR and ER function potentially contribute to the origin of numerous neurodegenerative diseases such as Alzheimer's and Parkinson's diseases [60].

As previously mentioned, DSS is a commonly used chemical to induce inflammation in the large intestines, providing a useful model for diseases like IBD. Even though it is evident that inflammation and ER stress significantly increase in the intestines after the DSS intake, the studies in the literature about the brain are limited to inflammation and neurogenesis in the various brain regions following the DSS treatment [47], [56]. Therefore, studying the IRE1 and its pro-apoptotic

downstream JNK as ER stress markers in the mouse cortical region is a novel attempt to observe the effects of the gut-brain axis on the ER stress in the brain.

This thesis aimed to investigate the activation of IRE1 and JNK signaling pathways as markers of ER stress in mouse cerebral cortex following DSS-added water intake. For this study, the mice were supplied with water and DSS-added water for 5 days. After the 5 days, mice were sacrificed, and the Western blot images were analyzed from the cerebral cortex tissue homogenates to investigate the effects of DSS intake on ER stress. For this purpose, the protein levels of IRE1 α, phosphorylated IRE1 (p-IRE1), the ratio of p-IRE1/IRE1, and JNK, phosphorylated JNK (p-JNK), the ratio of p-JNK/JNK in the cerebral cortex of mice were studied.

The findings from this study indicate no significant differences in the expression levels of IRE1, p-IRE1, or the p-IRE1/IRE1 ratio, nor JNK, p-JNK, or the p-JNK/JNK ratio between DSS-treated and control groups in the mouse cortex. These results are surprising, as DSS-induced colitis has been shown to cause systemic inflammation and has been associated with ER stress responses in tissues like the intestinal epithelium and inflammation in other brain regions such as the hippocampus [47], [61]. Therefore, we were expecting an increase in the p-IRE1/IRE1 and p-JNK/JNK levels to observe the phosphorylation and activation of ER stress in the cerebral cortex. Despite expectations, the cortical tissue in this study did not exhibit a measurable activation of the IRE1-JNK pathway under the experimental conditions employed.

A key consideration is the potential for tissue-specific differences in the susceptibility to DSS-induced ER stress. This experiment was initially designed by another laboratory to study large intestines, as DSS directly impacts the gut epithelium by disrupting the mucosal barrier and inducing immune responses [62]. DSS has a high molecular weight, which makes it unable to cross the blood-brain barrier (BBB). Nevertheless, DSS-induced colitis has been shown to mildly disrupt BBB integrity, leading to increased serum cytokine levels and secondary inflammation in the brain [63]. The lack of cortical ER stress activation can be explained by the resilience and neuroprotection mechanisms that might prevent ER stress activation under the subthreshold stress conditions in the brain.

Moreover, the colon hosts a diverse array of cell types with various functions, such as epithelial cells, immune cells, and enteric neurons. Among them, secretory cells such as Paneth cells and Goblet cells are especially affected by ER stress due to their critical role in producing and secreting large amounts of peptides, which makes them highly sensitive to disruptions in protein folding and processing [49]. Additionally, 70-80% of the intestinal cells consist of epithelial cells called enterocytes. These cells exhibit high regeneration potential and replenish every 1-5 days to provide healthy functioning of the colon. On the other hand, the cortex mainly consists of neurons, glial cells, and endothelial and perivascular cells. Neurons have evolved specific adaptations to cope with ER stress, given their high metabolic activity, reliance on proper protein folding for neurotransmission, and limited regenerative capacity [64]. Even though both neurons in the brain and intestinal cells possess mechanisms to manage ER stress, the efficiency and

outcomes of these mechanisms can differ between diverse cell types due to their unique functions and environments.

Another plausible explanation for the observed results is the diverse durations of activation of individual UPR arms. While all UPR branches are simultaneously activated within hours as a response to the ER stress, IRE1 signaling is the first one to return to its basal levels within a day. Hence, IRE1 activation peaks during early ER stress. Similarly, the activity of ATF4 is inhibited by negative feedback loops, and its activity reduces within two days [65]. In contrast, IRE1 signaling can trigger an increased PERK activation during prolonged stress [66]. In a similar manner, activation of JNK is rapid in response to ER stress, but the phosphorylated JNK levels diminish over time, following a trend that is parallel to the IRE1 [67]. Therefore, the 5-day DSS exposure period in this study may have been too prolonged to capture the transient peak of IRE1 and JNK activation, as the pathway might have returned to baseline levels by the time of tissue collection.

On the other hand, it is also possible that 5 days of DSS treatment may be insufficient to detect significant changes in the brain. Systemic inflammation resulting from DSS-induced colitis may require a longer duration to disrupt the BBB and initiate secondary inflammatory or ER stress responses in the brain. It has been known that chronic inflammation or prolonged exposure to inflammatory cytokines is often necessary to elicit measurable changes in brain ER stress markers, especially in regions like the cortex. Hence, it should be considered that the 5 days

of DSS exposure period in this study might have been too short to observe ER stress in the cortex [47].

An additional factor to consider is the potential for survivors' bias. When UPR fails to restore ER homeostasis and cellular homeostasis in case of prolonged stress, apoptotic pathways are initiated by the UPR. Under sustained ER stress, IRE1 can activate apoptotic signaling through the JNK pathway, which promotes the pro-apoptotic factors in cells [45]. In the context of our study, if a subset of cortical neurons experienced significant ER stress leading to apoptosis, these cells would no longer be present at the time of analysis. Consequently, the remaining cell population would predominantly consist of cells that either did not experience substantial ER stress or successfully adapted to it. This scenario could result in the observed non-significant IRE1 and JNK activation levels, as the apoptotic cells with elevated IRE1 and JNK markers would have been eliminated.

As mentioned above, the cortex is a highly heterogeneous structure that consists of various cell types, comprising not only neurons but also non-neuronal cells such as astrocytes, microglia, and oligodendrocytes, as well as different subregions [68]. Since the protein isolation was conducted from the whole cerebral cortex, the lack of regional or cellular separation in this study may have resulted in a dilution of any localized or cell type specific ER stress signals, as distinct cortical subregions as well as non-neuronal cells could exhibit differential activation of the IRE1-JNK pathway.

A common method used for DSS induction involves providing DSS in drinking water, allowing for continuous exposure. However, this approach could have led to variability in individual intake due to differences in drinking behavior among mice, potentially resulting in inconsistent dosing and heterogeneous disease severity in this study. Oral gavage is an alternative method that ensures uniform exposure across subjects by providing precise control over DSS dosage [69]. While this method can lead to more consistent experimental outcomes, it also introduces procedural stress that could confound results, especially in studies examining ER stress parameters. Similarly, individual housing can induce isolation stress, potentially affecting physiological and behavioral responses since mice are inherently social animals [70]. Therefore, the DSS administration in drinking water with individual housing while implementing enriched environments or allowing visual, auditory, and olfactory contact between individually housed mice might be the best scenario for reducing individual variability for DSS exposure.

Additionally, according to the Kruskal-Wallis and one-way ANOVA test, there were no significant increases or decreases in the expression of IRE1α, p-IRE1, p-IRE/IRE1, p-JNK, p-JNK/JNK in between control, DSS-treatment and recovery groups. The only significant increase is observed in the expression of JNK between the control and recovery groups (Figure A.1). However, to accurately assess JNK activation, the p-JNK/JNK should be considered rather than total JNK expression levels alone. Therefore, without a concurrent control group sacrificed on the same day as the recovery group, it is difficult to rule out time-related variations in JNK levels.

As well as parametric and non-parametric tests, correlation analysis and discrimination analysis were also performed to better understand the data. The pairwise relationship between six groups, p-IRE1/IRE1, IRE1, p-IRE1, p-JNK/JNK, JNK, and p-JNK, was investigated by performing a correlational analysis. The first correlation analysis examines the relationship of all protein expressions without considering group distinctions, while the other two correlation analyses are within control and treatment groups, respectively. Then, two linear discriminant analyses (LDA) were performed to explore the separability between the control and DSS-Treatment groups based on protein expression levels and their ratios. The first LDA was conducted between IRE1, p-IRE1, JNK, and p-JNK, while the second LDA focused exclusively on the ratios of p-IRE1/IRE1 and p-JNK/JNK between groups.

It was expected to observe strong correlations between the ratio of p-IRE1/IRE1 and IRE1α in all conditions and significant negative correlations were observed in overall and DSS-Treatment datasets. On the other hand, the correlation between p-IRE1/IRE1 and IRE1α in the control group is weaker, which suggests an inverse relationship without DSS treatment. Another positive significant correlation can be observed between p-JNK/JNK and p-JNK in all three correlation groups, which suggests that the treatment condition has no effect on this correlation. Additionally, the final significant correlation is between IRE1α and p-JNK in the overall dataset, which is a moderate one. This can be explained by the limited crosstalk between IRE1 and JNK pathways [71]. Interestingly, while the control group also demonstrates a moderate correlation between IRE1α and p-JNK, this shifts in the DSS-treated group to a correlation between p-IRE1 and JNK. The finding suggests a

potential shift in pathway dynamics under DSS-induced conditions, where the phosphorylation of IRE1 may associate more with JNK signaling.

The results of the first LDA, as shown in Table 11, indicate that JNK has the highest percentage contribution, which suggests that JNK is the dominant variable driving the distinction between the control and DSS-Treatment groups. While p-JNK plays a less significant role than JNK, IRE1α has the smallest contribution, signifying minimal influence on group separation. Also, p-IRE1 shows a negative coefficient, which indicates its opposing influence in the discriminative function.

In the second LDA, where only the ratios of p-IRE1/IRE1 and p-JNK/JNK were used, both of the coefficients are negative. The negative direction means that the higher values of these features are associated with a lower probability of belonging to the DSS-Treatment group. The p-JNK/JNK has a slightly stronger coefficient compared to p-IRE1/IRE1, so similar to the first LDA, JNK has a slightly stronger influence in separating the groups.

Overall, the inability to achieve separability of control and DSS-treatment groups in both analyses. This outcome aligns with the complexity of ER stress responses and supports earlier findings that the IRE1-JNK pathway did not exhibit significant activation in the cortex under DSS treatment.

Chapter 5

Conclusion & Future Directions

Overall, this thesis aims to explore the effects of DSS intake on ER stress and UPR signaling, focusing on the IRE1 and JNK pathways in the mouse cerebral cortex. Contrary to expectations, we observed no significant difference in the expression levels of IRE1, p-IRE1, and the p-IRE1/IRE1 ratio, as well as JNK, p-JNK, and the p-JNK/JNK ratio between control and DSS-Treatment groups. Additionally, the correlation analysis demonstrated a significant relationship between p-IRE1/IRE1 and IRE1α and between p-JNK/JNK and p-JNK, which was expected. The LDA failed to achieve clear separability between control and DSS-Treatment groups, which is a finding that supports the lack of significance in the expression levels. These findings suggest that DSS-induced IBD did not elicit a detectable ER stress response in the mouse cortex under the employed experimental conditions.

While the results did not indicate significant activation of the IRE1 or JNK pathways in the cortex under DSS treatment, this study represents a novel investigation into ER stress dynamics in the brain in the context of DSS-induced colitis. By exploring the potential effects of intestinal inflammation on neural ER stress pathways, this research contributes to the growing understanding of gut-brain interactions.

Although this study did not observe the effects of acute episodes on brain ER stress pathways, prolonged or severe intestinal inflammation could pose risks for neuroinflammatory conditions [72]. This study is an important baseline for future research into the effects of intestinal inflammation on brain health in gastrointestinal diseases. Prolonged or severe intestinal inflammation, as seen in chronic colitis, has been implicated in the development of neuroinflammatory conditions, which is a contributing factor in various neurodegenerative diseases [73]. Therefore, it is crucial to investigate ER stress pathways through which chronic intestinal diseases affect the brain. Understanding these mechanisms will aid in developing targeted therapeutic strategies for patients with IBD.

However, several limitations should be acknowledged to provide a comprehensive perspective on the findings and guide future research directions.

Although there is strong evidence from previous studies that DSS induction triggers intestinal inflammation and activates ER stress in the intestines [74], this study focused on the cortex and did not measure ER stress or inflammatory markers in the large intestine. Measuring ER stress and inflammatory markers in the intestine alongside the cortex would have enriched the findings and would have enabled a better understanding of the gut-brain axis in the context of DSS-induced colitis.

As mentioned in the discussion part, the IRE1 signaling branch is the first one to return to its basal levels through negative feedback loops within a day and JNK follows a similar timeline [75]. Instead of checking ER stress only at a single time point on day 5, analyzing ER stress markers at multiple time points, such as each

day up to 5 days, can provide more understanding of the activation and attenuation patterns of IRE1 and JNK pathways.

Additionally, this study investigated the effects of acute DSS treatment. To gain more insight into how DSS-induced gastrointestinal diseases affect the brain in the long term, chronic or relapsing mouse models can be utilized. These models could provide valuable insights into the broader impact of systemic inflammation on neurobiology, including potential cumulative or adaptive effects over time.

This study focused on the IRE1 branch of the UPR, while PERK and ATF6 pathways were not investigated. The three UPR branches show crosstalk between each other and adjust the cellular response to ER together. For instance, activation of ATF6 can upregulate BIP, which is an ER chaperone that modulates the activity of both IRE1 and PERK, thereby influencing their signaling outputs [76]. Therefore, evaluating the PERK and ATF6 pathways alongside IRE1 to capture the full spectrum of the UPR could be important for future studies.

Moreover, activation of IRE1 leads to two main downstream signaling pathways. While the activation of XBP1 promotes cell survival at the early stages of ER stress, activation of JNK downstream induces apoptosis in prolonged or severe stress [77]. The XBP1 antibody that was tried in this experiment was not suitable for use in the brain tissues. However, checking both downstream pathways can provide complementary insight into the cell fate determination of ER stress.

ER stress and inflammation often show comorbidity, with ER stress serving both as a trigger and a consequence of inflammatory pathways [78]. In the DSS-induced

colitis model, increased intestinal permeability causes systemic inflammation, which damages the BBB [48]. Hence, checking inflammatory markers with ER stress markers, along with checking the BBB integrity might provide a better explanation for nonsignificant IRE1 and JNK results.

Furthermore, cells with high ER stress could have undergone apoptosis due to prolonged stress [79]. As explained in the discussion section, it could be the reason why there was no activation in IRE1 and JNK. Thus, the inclusion of apoptotic assays, such as TUNEL staining or cleaved caspase-3 detection by immunohistochemistry or western blot, could provide insights into whether ER stress-induced apoptosis influenced the observed results.

This study exclusively used male mice, which may limit the generalizability of the findings to female populations. Female mice often exhibit more robust immune responses, including heightened cytokine production [80], which could amplify the systemic effects of DSS-induced colitis on the brain. Hence, including female mice in future experiments would provide a more comprehensive understanding of how gender influences the gut-brain axis under DSS treatment.

While this study focuses on the effects of DSS-induced colitis in ER stress pathways in the cortex, the diet and age of the mouse animal model should be considered carefully. In this study, a standard chow diet was given to the animals, whereas human diets, especially Western diets, have higher fat content than a standard diet. Additionally, using a limited age group may limit the findings for diseases like IBD, which is a lifelong disease. Hence, to enhance the translational value of the findings,

future experimental designs should carefully consider dietary compositions and age-related factors.

Lastly, this study focused on the cortex, but other brain regions, such as the hippocampus or hypothalamus, may respond differently to DSS-induced colitis. Previous studies have observed altered neurogenesis and inflammation markers in the hippocampus after DSS treatment [56], [81]. As well as changes in molecular and behavioral stress responses, which occur in the hippocampus and hypothalamus of the DSS-induced colitis mouse model [82]. These findings indicate two different future directions; the first one is the importance of examining multiple brain regions to fully understand the impact of colitis on the central nervous system, and the second one is that behavioral assessments help elucidate region-specific effects of ER stress, as the hippocampus and prefrontal cortex are key regions involved in mood and cognition.

Bibliography

[1] D. S. Schwarz and M. D. Blower, “The endoplasmic reticulum: structure, function and response to cellular signaling,” *Cell Mol Life Sci*, vol. 73, no. 1, p. 79, Jan. 2015, doi: 10.1007/S00018-015-2052-6.

[2] B. Alberts, A. Johnson, J. Lewis, M. Raff, K. Roberts, and P. Walter, “The Endoplasmic Reticulum,” 2002, Accessed: Dec. 16, 2024. [Online]. Available: https://www.ncbi.nlm.nih.gov/books/NBK26841/

[3] B. G. Spencer and J. W. Finnie, “The Role of Endoplasmic Reticulum Stress in Cell Survival and Death,” *J Comp Pathol*, vol. 181, pp. 86–91, Nov. 2020, doi: 10.1016/J.JCPA.2020.10.006.

[4] B. M. Carlson, “Cells,” in *The Human Body*, Academic Press, 2019, pp. 1–25. doi: 10.1016/B978-0-12-804254-0.00001-6.

[5] B. Alberts, A. Johnson, J. Lewis, M. Raff, K. Roberts, and P. Walter, “The Endoplasmic Reticulum,” in *Molecular Biology of the Cell*, 4th ed., Garland Science, 2002. Accessed: Dec. 17, 2024. [Online]. Available: https://www.ncbi.nlm.nih.gov/books/NBK26841/

[6] “Endoplasmic reticulum (ER) | Definition, Function, & Location | Britannica.” Accessed: Dec. 16, 2024. [Online]. Available: https://www.britannica.com/science/endoplasmic-reticulum

[7] J. G. Burr, “Tools of the Cell Biologist,” in *Medical Cell Biology: Third Edition*, Academic Press, 2008, pp. 1–26. doi: 10.1016/B978-0-12-370458-0.50006-2.

[8] R. B. Sher, G. A. Cox, and C. Ackert-Bicknell, “Development and Disease of Mouse Muscular and Skeletal Systems,” in *The Laboratory Mouse*, Academic Press, 2012, pp. 209–239. doi: 10.1016/B978-0-12-382008-2.00010-6.

[9] M. J. Phillips and G. K. Voeltz, “Structure and function of ER membrane contact sites with other organelles,” 2016. doi: 10.1038/nrm.2015.8.

[10] C. H. Jan, C. C. Williams, and J. S. Weissman, “Principles of ER cotranslational translocation revealed by proximity-specific ribosome profiling,” *Science (1979)*, vol. 346, no. 6210, Nov. 2014, doi: 10.1126/SCIENCE.1257521/SUPPL_FILE/REVISION1_MS1257521TABLES6.TXT.

[11] R. Gilmore, G. Blobel, and P. Walter, “Protein translocation across the endoplasmic reticulum. I. Detection in the microsomal membrane of a receptor for the signal recognition particle.,” *Journal of Cell Biology*, vol. 95, no. 2, pp. 463–469, Nov. 1982, doi: 10.1083/JCB.95.2.463.

[12] I. Braakman and D. N. Hebert, “Protein Folding in the Endoplasmic Reticulum,” *Cold Spring Harb Perspect Biol*, vol. 5, no. 5, p. a013201, May 2013, doi: 10.1101/CSHPERSPECT.A013201.

[13] D. N. Hebert and M. Molinari, “In and out of the ER: Protein folding, quality control, degradation, and related human diseases,” *Physiol Rev*, vol. 87, no. 4, pp. 1377–1408, Oct. 2007, doi: 10.1152/PHYSREV.00050.2006/ASSET/IMAGES/LARGE/Z9J0040724410005.JPEG.

[14] A. Ruggiano, O. Foresti, and P. Carvalho, “ER-associated degradation: Protein quality control and beyond,” *Journal of Cell Biology*, vol. 204, no. 6, pp. 869–879, Mar. 2014, doi: 10.1083/JCB.201312042.

[15] B. Meusser, C. Hirsch, E. Jarosch, and T. Sommer, “ERAD: the long road to destruction,” *Nature Cell Biology 2005 7:8*, vol. 7, no. 8, pp. 766–772, Aug. 2005, doi: 10.1038/ncb0805-766.

[16] P. Fagone and S. Jackowski, “Membrane phospholipid synthesis and endoplasmic reticulum function,” *J Lipid Res*, vol. 50, no. SUPPL., pp. S311–S316, Apr. 2009, doi: 10.1194/JLR.R800049-JLR200.

[17] M. S. Brown and J. L. Goldstein, “A proteolytic pathway that controls the cholesterol content of membranes, cells, and blood,” *Proc Natl Acad Sci U S A*, vol. 96, no. 20, pp. 11041–11048, Sep. 1999, doi: 10.1073/PNAS.96.20.11041/ASSET/9D6BBDF0-0345-4E3D-9745-776A6BD5182E/ASSETS/GRAPHIC/PQ1992882005.JPEG.

[18] J. Groenendyk, L. B. Agellon, and M. Michalak, “Calcium signaling and endoplasmic reticulum stress,” *Int Rev Cell Mol Biol*, vol. 363, pp. 1–20, Jan. 2021, doi: 10.1016/BS.IRCMB.2021.03.003.

[19] M. Endo, “Calcium-induced calcium release in skeletal muscle,” *Physiol Rev*, vol. 89, no. 4, pp. 1153–1176, Oct. 2009, doi: 10.1152/PHYSREV.00040.2008/ASSET/IMAGES/LARGE/Z9J0040925230003.JPEG.

[20] M. D. Bootman, “Calcium Signaling,” *Cold Spring Harb Perspect Biol*, vol. 4, no. 7, p. a011171, Jul. 2012, doi: 10.1101/CSHPERSPECT.A011171.

[21] S. S. Vembar and J. L. Brodsky, “One step at a time: endoplasmic reticulum-associated degradation,” *Nat Rev Mol Cell Biol*, vol. 9, no. 12, pp. 944–957, Dec. 2008, doi: 10.1038/NRM2546.

[22] L. Ozcan and I. Tabas, “Role of endoplasmic reticulum stress in metabolic disease and other disorders,” *Annu Rev Med*, vol. 63, no. Volume 63, 2012, pp. 317–328, Feb. 2012, doi: 10.1146/ANNUREV-MED-043010-144749/CITE/REFWORKS.

[23] Y. Liu, C. Xu, R. Gu, R. Han, Z. Li, and X. Xu, “Endoplasmic reticulum stress in diseases,” *MedComm (Beijing)*, vol. 5, no. 9, p. e701, Sep. 2024, doi: 10.1002/MCO2.701.

[24] I. L. Lemmer, N. Willemsen, N. Hilal, and A. Bartelt, “A guide to understanding endoplasmic reticulum stress in metabolic disorders,” *Mol Metab*, vol. 47, p. 101169, May 2021, doi: 10.1016/J.MOLMET.2021.101169.

[25] D. J. Todd, A. H. Lee, and L. H. Glimcher, “The endoplasmic reticulum stress response in immunity and autoimmunity,” *Nature Reviews Immunology 2008 8:9*, vol. 8, no. 9, pp. 663–674, Sep. 2008, doi: 10.1038/nri2359.

[26] M. C. Kopp, N. Larburu, V. Durairaj, C. J. Adams, and M. M. U. Ali, “UPR proteins IRE1 and PERK switch BiP from chaperone to ER stress sensor,” *Nature Structural & Molecular Biology 2019 26:11*, vol. 26, no. 11, pp. 1053–1062, Nov. 2019, doi: 10.1038/s41594-019-0324-9.

[27] M. A. Lloyd, J. C. Osborne, B. Safer, G. M. Powell, and W. C. Merrick, “Characteristics of eukaryotic initiation factor 2 and its subunits.,” *Journal of Biological Chemistry*, vol. 255, no. 3, pp. 1189–1193, Feb. 1980, doi: 10.1016/S0021-9258(19)86161-6.

[28] N. Hiramatsu, C. Messah, J. Han, M. M. LaVail, R. J. Kaufman, and J. H. Lin, “Translational and posttranslational regulation of XIAP by eIF2α and ATF4 promotes ER stress-induced cell death during the unfolded protein response,” *Mol Biol Cell*, vol. 25, no. 9, pp. 1411–1420, May 2014, doi: 10.1091/MBC.E13-11-0664/ASSET/IMAGES/LARGE/1411FIG7.JPEG.

[29] C. Hetz, “The unfolded protein response: controlling cell fate decisions under ER stress and beyond,” *Nature Reviews Molecular Cell Biology 2012 13:2*, vol. 13, no. 2, pp. 89–102, Jan. 2012, doi: 10.1038/nrm3270.

[30] A. Gorman *et al.*, “Current Concepts in ER Stress-Induced Apoptosis Article in Journal of Carcinogenesis & Mutagenesis ·,” 2013, doi: 10.4172/2157-2518.S6-002.

[31] T. Iwawaki *et al.*, “Translational control by the ER transmembrane kinase/ribonuclease IRE1 under ER stress,” *Nature Cell Biology 2001 3:2*, vol. 3, no. 2, pp. 158–164, Jan. 2001, doi: 10.1038/35055065.

[32] A. Bertolotti *et al.*, “Increased sensitivity to dextran sodium sulfate colitis in IRE1beta-deficient mice,” *J Clin Invest*, vol. 107, no. 5, pp. 585–593, 2001, doi: 10.1172/JCI11476.

[33] M. Khanna, N. Agrawal, R. Chandra, and G. Dhawan, “Targeting unfolded protein response: a new horizon for disease control,” *Expert Rev Mol Med*, vol. 23, p. e1, 2021, doi: 10.1017/ERM.2021.2.

[34] D. Ron and S. R. Hubbard, “How IRE1 reacts to ER stress,” *Cell*, vol. 132, no. 1, pp. 24–26, Jan. 2008, doi: 10.1016/J.CELL.2007.12.017.

[35] B. M. Gardner and P. Walter, “Unfolded proteins are Ire1-activating ligands that directly induce the unfolded protein response,” *Science*, vol. 333, no. 6051, pp. 1891–1894, Sep. 2011, doi: 10.1126/SCIENCE.1209126.

[36] H. Yoshida, T. Matsui, A. Yamamoto, T. Okada, and K. Mori, “XBP1 mRNA is induced by ATF6 and spliced by IRE1 in response to ER stress to produce a highly active transcription factor,” *Cell*, vol. 107, no. 7, pp. 881–891, Dec. 2001, doi: 10.1016/S0092-8674(01)00611-0.

[37] A. Almanza *et al.*, “Endoplasmic reticulum stress signalling – from basic mechanisms to clinical applications,” *FEBS J*, vol. 286, no. 2, pp. 241–278, Jan. 2019, doi: 10.1111/FEBS.14608.

[38] P. Kimmig *et al.*, "The unfolded protein response in fission yeast modulates stability of select mRNAs to maintain protein homeostasis," *Elife*, vol. 2012, no. 1, Oct. 2012, doi: 10.7554/ELIFE.00048.

[39] K. I. Mishiba *et al.*, "Defects in IRE1 enhance cell death and fail to degrade mRNAs encoding secretory pathway proteins in the Arabidopsis unfolded protein response," *Proc Natl Acad Sci U S A*, vol. 110, no. 14, pp. 5713–5718, Apr. 2013, doi: 10.1073/PNAS.1219047110/SUPPL_FILE/SD02.XLS.

[40] F. Urano *et al.*, "Coupling of stress in the ER to activation of JNK protein kinases by transmembrane protein kinase IRE1," *Science*, vol. 287, no. 5453, pp. 664–666, Jan. 2000, doi: 10.1126/SCIENCE.287.5453.664.

[41] M. S. Uddin, W. S. Yu, and L. W. Lim, "Exploring ER stress response in cellular aging and neuroinflammation in Alzheimer's disease," *Ageing Res Rev*, vol. 70, p. 101417, Sep. 2021, doi: 10.1016/J.ARR.2021.101417.

[42] R. P. Junjappa, P. Patil, K. R. Bhattarai, H. R. Kim, and H. J. Chae, "IRE1α implications in endoplasmic reticulum stress-mediated development and pathogenesis of autoimmune diseases," *Front Immunol*, vol. 9, no. JUN, p. 362725, Jun. 2018, doi: 10.3389/FIMMU.2018.01289/BIBTEX.

[43] L. Weiss, A. J. Whitmarsh, D. D. Yang, M. Rincón, R. J. Davis, and R. A. Flavell, "Regulation of c-Jun NH2-terminal Kinase (Jnk) Gene Expression during T Cell Activation," *J Exp Med*, vol. 191, no. 1, p. 139, Jan. 2000, doi: 10.1084/JEM.191.1.139.

[44] T. S. Fung, Y. Liao, and D. X. Liu, “The Endoplasmic Reticulum Stress Sensor IRE1α Protects Cells from Apoptosis Induced by the Coronavirus Infectious Bronchitis Virus,” *J Virol*, vol. 88, no. 21, pp. 12752–12764, Nov. 2014, doi: 10.1128/JVI.02138-14/ASSET/3DB2DFDD-B5CF-4E92-BC5A-C0B994141CD4/ASSETS/GRAPHIC/ZJV9990996820007.JPEG.

[45] R. Sano and J. C. Reed, “ER stress-induced cell death mechanisms,” *Biochim Biophys Acta*, vol. 1833, no. 12, pp. 3460–3470, Dec. 2013, doi: 10.1016/J.BBAMCR.2013.06.028.

[46] N. Siwecka, W. Rozpędek-Kamińska, A. Wawrzynkiewicz, D. Pytel, J. A. Diehl, and I. Majsterek, “The Structure, Activation and Signaling of IRE1 and Its Role in Determining Cell Fate,” *Biomedicines 2021, Vol. 9, Page 156*, vol. 9, no. 2, p. 156, Feb. 2021, doi: 10.3390/BIOMEDICINES9020156.

[47] Y. Han *et al.*, “Cortical Inflammation is Increased in a DSS-Induced Colitis Mouse Model,” *Neurosci Bull*, vol. 34, doi: 10.1007/s12264-018-0288-5.

[48] S. Talley, R. Valiauga, L. Anderson, A. R. Cannon, M. A. Choudhry, and E. M. Campbell, “DSS-induced inflammation in the colon drives a proinflammatory signature in the brain that is ameliorated by prophylactic treatment with the S100A9 inhibitor paquinimod,” *J Neuroinflammation*, vol. 18, no. 1, pp. 1–14, Dec. 2021, doi: 10.1186/S12974-021-02317-6/FIGURES/5.

[49] A. Kaser and R. S. Blumberg, “Endoplasmic reticulum stress and intestinal inflammation,” *Mucosal Immunol*, vol. 3, no. 1, pp. 11–16, Jan. 2010, doi: 10.1038/MI.2009.122.

[50] A. Kaser and R. S. Blumberg, “Autophagy, Microbial Sensing, Endoplasmic Reticulum Stress, and Epithelial Function in Inflammatory Bowel Disease,” *Gastroenterology*, vol. 140, no. 6, pp. 1738-1747.e2, May 2011, doi: 10.1053/J.GASTRO.2011.02.048.

[51] M. Perše and A. Cerar, “Dextran Sodium Sulphate Colitis Mouse Model: Traps and Tricks,” *Biomed Res Int*, vol. 2012, no. 1, p. 718617, Jan. 2012, doi: 10.1155/2012/718617.

[52] “Why Animal Research? | Animal Research at Stanford | Stanford Medicine.” Accessed: Jan. 21, 2025. [Online]. Available: https://med.stanford.edu/animalresearch/why-animal-research.html?utm_source=chatgpt.com

[53] S. D. Forssten, A. C. Ouwehand, S. M. Griffin, and E. Patterson, “One Giant Leap from Mouse to Man: The Microbiota–Gut–Brain Axis in Mood Disorders and Translational Challenges Moving towards Human Clinical Trials,” *Nutrients 2022, Vol. 14, Page 568*, vol. 14, no. 3, p. 568, Jan. 2022, doi: 10.3390/NU14030568.

[54] J. Burisch, T. Jess, M. Martinato, and P. L. Lakatos, “The burden of inflammatory bowel disease in Europe,” *J Crohns Colitis*, vol. 7, no. 4, pp. 322–337, May 2013, doi: 10.1016/J.CROHNS.2013.01.010.

[55] F. Reichmann, A. M. Hassan, A. Farzi, P. Jain, R. Schuligoi, and P. Holzer, "Dextran sulfate sodium-induced colitis alters stress-associated behaviour and neuropeptide gene expression in the amygdala-hippocampus network of mice," *Scientific Reports 2015 5:1*, vol. 5, no. 1, pp. 1–13, Jun. 2015, doi: 10.1038/srep09970.

[56] S. Zonis *et al.*, "Chronic intestinal inflammation alters hippocampal neurogenesis," *J Neuroinflammation*, vol. 12, no. 1, p. 65, Apr. 2015, doi: 10.1186/S12974-015-0281-0.

[57] T. Mahmood and P. C. Yang, "Western Blot: Technique, Theory, and Trouble Shooting," *N Am J Med Sci*, vol. 4, no. 9, p. 429, Sep. 2012, doi: 10.4103/1947-2714.100998.

[58] S. Stael, L. P. Miller, Á. D. Fernández-Fernández, and F. Van Breusegem, "Detection of Damage-Activated Metacaspase Activity by Western Blot in Plants," *Methods in Molecular Biology*, vol. 2447, pp. 127–137, 2022, doi: 10.1007/978-1-0716-2079-3_11/FIGURES/1.

[59] C. Hetz and S. Saxena, "ER stress and the unfolded protein response in neurodegeneration," *Nature Reviews Neurology 2017 13:8*, vol. 13, no. 8, pp. 477–491, Jul. 2017, doi: 10.1038/nrneurol.2017.99.

[60] W. Scheper and J. J. M. Hoozemans, "The unfolded protein response in neurodegenerative diseases: a neuropathological perspective," *Acta Neuropathol*, vol. 130, no. 3, pp. 315–331, Sep. 2015, doi: 10.1007/S00401-015-1462-8/FIGURES/3.

[61] J. S. Boles *et al.*, "A leaky gut dysregulates gene networks in the brain associated with immune activation, oxidative stress, and myelination in a mouse model of colitis," *Brain Behav Immun*, vol. 117, pp. 473–492, Mar. 2024, doi: 10.1016/J.BBI.2024.02.007.

[62] S. Jamwal and P. Kumar, "Animal Models of Inflammatory Bowel Disease," in *Animal Models for the Study of Human Disease: Second Edition*, Second Edition., Academic Press, 2017, ch. 19, pp. 467–477. doi: 10.1016/B978-0-12-809468-6.00019-X.

[63] Z. J. Wang, L. H. Chen, J. Xu, Q. X. Xu, W. Xu, and X. W. Yang, "Corylin ameliorates chronic ulcerative colitis via regulating the gut–brain axis and promoting 5-hydroxytryptophan production in the colon," *Phytomedicine*, vol. 110, p. 154651, Feb. 2023, doi: 10.1016/J.PHYMED.2023.154651.

[64] K. Wolzak *et al.*, " Neuron-specific translational control shift ensures proteostatic resilience during ER stress ," *EMBO J*, vol. 41, no. 16, p. 110501, Aug. 2022, doi: 10.15252/EMBJ.2021110501/SUPPL_FILE/EMBJ2021110501-SUP-0010-SDATAEV.ZIP.

[65] H. D. Ryoo, "Long and short (timeframe) of endoplasmic reticulum stress-induced cell death," *FEBS J*, vol. 283, no. 20, p. 3718, Oct. 2016, doi: 10.1111/FEBS.13755.

[66] G. Ong, R. Ragetli, K. Mnich, B. W. Doble, W. Kammouni, and S. E. Logue, "IRE1 signaling increases PERK expression during chronic ER stress," *Cell*

Death & Disease 2024 15:4, vol. 15, no. 4, pp. 1–11, Apr. 2024, doi: 10.1038/s41419-024-06663-0.

[67] J. H. Lin *et al.*, "IRE1 signaling affects cell fate during the unfolded protein response," *Science (1979)*, vol. 318, no. 5852, pp. 944–949, Nov. 2007, doi: 10.1126/SCIENCE.1146361/ASSET/032876C0-0229-4CF0-8D61-B7D42A42F079/ASSETS/GRAPHIC/318_944_F5.JPEG.

[68] B. V. der Garabedian and J. Mariani, "Gap Junctions in Cerebellar Development and Pathology," in *Gap Junctions in the Brain: Physiological and Pathological Roles*, Academic Press, 2013, ch. 11, pp. 189–200. doi: 10.1016/B978-0-12-415901-3.00011-6.

[69] D. Wang, W. Chen, J. Cao, L. Si, and Z. Chen, "Establishment and Evaluation of a Mouse Model of Experimental Ulcerative Colitis Induced by the Gavage Administration of Dextran Sulfate Sodium," *Biomedicines*, vol. 12, no. 8, p. 1764, Aug. 2024, doi: 10.3390/BIOMEDICINES12081764.

[70] S. S. Arndt *et al.*, "Individual housing of mice--impact on behaviour and stress responses," *Physiol Behav*, vol. 97, no. 3–4, pp. 385–393, Jun. 2009, doi: 10.1016/J.PHYSBEH.2009.03.008.

[71] D. Pinkaew *et al.*, "Fortilin binds IRE1α and prevents ER stress from signaling apoptotic cell death," *Nature Communications 2017 8:1*, vol. 8, no. 1, pp. 1–16, May 2017, doi: 10.1038/s41467-017-00029-1.

[72] S. E. Lakhan and A. Kirchgessner, “Neuroinflammation in inflammatory bowel disease,” *J Neuroinflammation*, vol. 7, p. 37, Jul. 2010, doi: 10.1186/1742-2094-7-37.

[73] W. Zhang, D. Xiao, Q. Mao, and H. Xia, “Role of neuroinflammation in neurodegeneration development,” *Signal Transduction and Targeted Therapy 2023 8:1*, vol. 8, no. 1, pp. 1–32, Jul. 2023, doi: 10.1038/s41392-023-01486-5.

[74] X. Ma *et al.*, “Intestinal Epithelial Cell Endoplasmic Reticulum Stress and Inflammatory Bowel Disease Pathogenesis: An Update Review,” *Front Immunol*, vol. 8, no. OCT, p. 1271, Oct. 2017, doi: 10.3389/FIMMU.2017.01271.

[75] F. Walter, J. Schmid, H. Dussmann, C. G. Concannon, and J. H. M. Prehn, “Imaging of single cell responses to ER stress indicates that the relative dynamics of IRE1/XBP1 and PERK/ATF4 signalling rather than a switch between signalling branches determine cell survival,” *Cell Death & Differentiation 2015 22:9*, vol. 22, no. 9, pp. 1502–1516, Jan. 2015, doi: 10.1038/cdd.2014.241.

[76] B. F. Teske *et al.*, “The eIF2 kinase PERK and the integrated stress response facilitate activation of ATF6 during endoplasmic reticulum stress,” *Mol Biol Cell*, vol. 22, no. 22, pp. 4390–4405, Nov. 2011, doi: 10.1091/MBC.E11-06-0510/ASSET/IMAGES/LARGE/4390FIG9.JPEG.

[77] Y. Chen and F. Brandizzi, “IRE1: ER stress sensor and cell fate executor,” *Trends Cell Biol*, vol. 23, no. 11, pp. 547–555, Nov. 2013, doi: 10.1016/J.TCB.2013.06.005.

[78] S. Z. Hasnain, R. Lourie, I. Das, A. C. H. Chen, and M. A. McGuckin, “The interplay between endoplasmic reticulum stress and inflammation,” *Immunol Cell Biol*, vol. 90, no. 3, pp. 260–270, Mar. 2012, doi: 10.1038/ICB.2011.112.

[79] I. Tabas and D. Ron, “Integrating the mechanisms of apoptosis induced by endoplasmic reticulum stress,” *Nature Cell Biology 2011 13:3*, vol. 13, no. 3, pp. 184–190, Mar. 2011, doi: 10.1038/ncb0311-184.

[80] S. L. Klein and K. L. Flanagan, “Sex differences in immune responses,” *Nature Reviews Immunology 2016 16:10*, vol. 16, no. 10, pp. 626–638, Aug. 2016, doi: 10.1038/nri.2016.90.

[81] J. Do and J. Woo, “From Gut to Brain: Alteration in Inflammation Markers in the Brain of Dextran Sodium Sulfate-induced Colitis Model Mice,” *Clinical Psychopharmacology and Neuroscience*, vol. 16, no. 4, pp. 422–433, Nov. 2018, doi: 10.9758/CPN.2018.16.4.422.

[82] F. Reichmann, A. M. Hassan, A. Farzi, P. Jain, R. Schuligoi, and P. Holzer, “Dextran sulfate sodium-induced colitis alters stress-associated behaviour and neuropeptide gene expression in the amygdala-hippocampus network of mice,” *Sci Rep*, vol. 5, p. 9970, Jun. 2015, doi: 10.1038/SREP09970.

Appendix A

A.1 Recovery Group Included Kruskal-Wallis and T-Test Results

The experimental design was determined and executed by Bahar Değirmenci Lab Group. The recovery group was given DSS-included water for 5 days, and then only water for 2 days. However, all the control group animals were sacrificed along with the DSS-Treatment group's animals, and the animals of the recovery group were sacrificed after 7 days. Hence, the recovery group was not included in the results and the data including this group was added as "Appendix A" part of the study.

A.1.1 The Effect of DSS Treatment on p-IRE1α and p-JNK in Mouse Cerebral Cortex with Recovery Group

The recovery group was also tested with control and DSS-Treatment groups. The phosphorylation levels of IRE1α and JNK were then determined by calculating the ratio of phosphorylated protein to total protein. Normality and heterogeneity of the data were checked by Shapiro-Wilk and Levene's Tests, respectively. There was no significance between the three groups of variables for p-IRE (p = 0,236) and p-JNK/JNK (p = 0.994) according to the Kruskal-Wallis Test. One-way ANOVA was applied to the remaining ones; p-IRE1/IRE1α ($F_{(x)}$ = 2.073, p = 0.160), IRE1α ($F_{(x)}$ = 0.404, p = 0.675), and p-JNK ($F_{(x)}$ = 1.324, p = 0.295) does not show any significant change. On the other hand, there is a significant increase ($F_{(x)}$ = 5.822, p = 0.013) in the recovery group compared to

the control for the JNK expression according to the Bonferroni test in post-hoc analysis. The graphs are added below to Figure A.1.

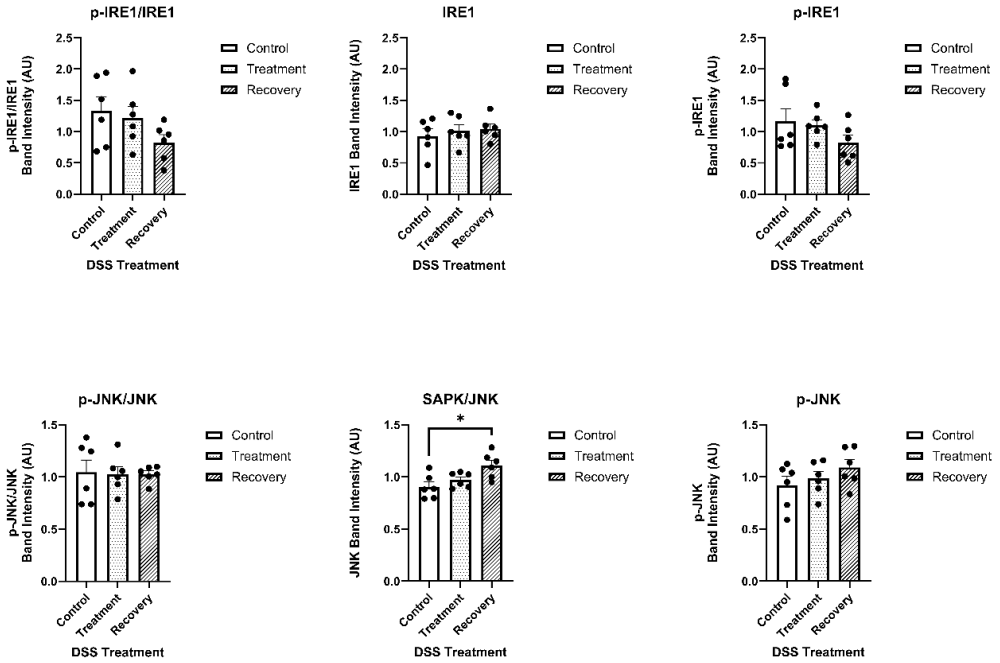

Figure A.1. Expression Levels of p-IRE/IRE1, IRE1, p-IRE1, p-JNK/JNK, JNK, and p-JNK across all groups in the Cerebral Cortex. The graph shows the normalized quantification of the p-IRE/IRE1α, IRE1, p-IRE1, p-JNK/JNK, JNK, and p-JNK for control, DSS-Treatment, and recovery groups, respectively. The error bars represent mean +1 SEM and statistical significance was set at $p < 0.05$. n=6 for all groups.